UNIVERSITY OF CALIFORNIA
RIVERSIDE

Development of a universal FRET technology for determining biochemical and pharmaceutical parameters and application in deciphering the interplay between influenza viruses and SUMOylation pathway

A Dissertation submitted in partial satisfaction
of the requirements for the degree of

Doctor of Philosophy

in

Bioengineering

by

Zhehao Xiong

September 2018

Dissertation Committee:
Dr. Jiayu Liao, Chairperson
Dr. Dimitrios Morikis
Dr. Jun Li

The Dissertation of Zhehao Xiong is approved:

_____

_____

_____

Committee Chairperson

University of California, Riverside

Acknowledgements

I would like to thank Dr. Jiayu Liao for his support and guidance across my PhD study, Dr. Shasha Zheng, Dr. Dimitrios Morikis and Dr. Jun Li for their helpful advice. I also thank all the members in Liao's group for their collaborative work and helpful discussion. Dr. Jiayu Liao supervised the research which forms the basis for this dissertation.

Dedication

I would like to dedicate this dissertation to my wife and parents for their constant support and encouragement throughout my PhD study.

ABSTRACT OF THE DISSERTATION

Development of a universal FRET technology for determining biochemical and pharmaceutical parameters and application in deciphering the interplay between influenza viruses and SUMOylation pathway

by

Zhehao Xiong

Doctor of Philosophy, Graduate Program in Bioengineering
University of California, Riverside, September 2018
Dr. Jiayu Liao, Chairperson

SUMOylation is one of the most important post-translational modifications, which plays pivotal roles in many physiological processes. SUMOylation is a multi-step enzymatic cascade, which involves multiple protein-protein interactions and regulates protein activity in many aspects. Misregulation of the SUMO pathway has been associated with many types of diseases, including viral infection, tumorigenesis, and neurodegenerative diseases. Thus, SUMOylation has great potential to be a target for the development of novel antiviral and anticancer agents. Förster Resonance Energy Transfer (FRET) is an energy transfer process that occurs between two interacting fluorophores with overlapping spectra, and is widely used to study protein-protein interactions. Previously, our group has developed quantitative FRET assay for determining protein interaction affinity and enzymatic kinetics. Here, my research goal is to further develop quantitative

FRET (qFRET) technology into a robust and reliable method for determining biochemical parameters, and to investigate the interplay between SUMOylation and influenza replication. Specifically, I have proven our high-sensitive FRET technology can be used to determine protein interaction affinity even without protein purification, and utilizing this strategy I have for the first time measured the K_d between SUMO E3-PIAS1 with SUMO E2 or SUMO substrate-NS1 which elucidates the mechanism of how SUMO E3 regulates SUMOylation of different substrates. Then, I have developed a systematic method for determining mechanism of enzyme inhibition through our qFRET technology, and characterized the inhibition type and inhibition constant of our newly found SUMOylation inhibitor- STE. We have also identified Lys131 of influenza NS1 protein as the SUMOylated lysine residue which is important for virus replication through an *in vitro* FRET-based SUMOylation assay. And lastly, I have shown our SUMOylation inhibitor-STE exhibits great inhibition on influenza growth and can serve as a potential new anti-influenza drug. In summary, these findings prove our qFRET technology provides a powerful tool for determining biochemical parameters and dissects the role of SUMOylation in influenza viral life cycle.

Table of contents

CHAPTER 1: INTRODUCTION 1

CHAPTER 2: Determine Protein Interaction Affinity Without Protein Purification by Quantitative FRET (qFRET) Technology 12

Abstract 12

Introduction 14

Materials and Methods 21

Results 27

Discussion 47

CHAPTER 3: Development of Quantitative FRET Technology for K_i Determination and its Application for Characterization of a Small Molecule Inhibitor of SUMOylation 51

Abstract 51

Introduction 52

Materials and Methods 57

Results 60

Discussion 70

CHAPTER 4: Discovery and Characterization of SUMOylation Site of NS1 Protein in Influenza Viral Life Cycle Using FRET Technology 72

Abstract 72

Introduction 73

Materials and Methods 76

Results 82

Discussion 99

References 103

List of Figures

Figure 1.1. Conjugation and deconjugation of SUMO to and from substrate proteins require multiples enzymes. 3

Figure 1.2. Inhibition of STAT1-mediated IFN-γ pathway by PIAS1, a SUMO E3 ligase. 6

Figure 1.3. Principle of FRET. 10

Figure 2.1. Quantitative spectrum analysis of FRET signal. 18

Figure 2.2. Schematic diagram of FRET-based assay for determination of protein interaction dissociation constant, K_d, in the presence of other proteins. 29

Figure 2.3. Fluorescence signal analysis and titration of FRET signal. 34

Figure 2.4. Em_{FRET} at different concentrations of purified CyPetRanGAP1c and YPetUbc9 in the presence or absence of other proteins. 36

Figure 2.5. SDS-PAGE protein gel of CyPetRanGAP1c and YPetUbc9 under different conditions. 40

Figure 2.6. EmFRETmax at different concentrations of the donor CyPetRanGAP1c in the absence and presence of other proteins. 44

Figure 2.7. Determination of interaction affinity K_d by surface plasma resonance. 45

Figure 3.1. A quantitative FRET assay to measure kinetics of the E1 enzyme in the SUMOylation pathway. 60

Figure 3.2. Equilibrium treatment of reversible inhibition. 63

Figure 3.3. STE inhibits SUMO E2 thioester formation in a dose dependent manner in vitro. 65

Figure 3.4. Enzyme kinetics of SUMO E1 in the absence and presence of different concentrations of STE. 68

Figure 4.1. Principle of FRET-based SUMOylation assay to determine SUMOylated lysine residues. 83

Figure 4.2. Establishment of the in vitro SUMOylation assay. 85

Figure 4.3. In vitro SUMOylation assay of all mutant YPetNS1. 88

Figure 4.4. Confirmation of the SUMOylation site of NS1 91

Figure 4.5. Generation of HA-pseudotyped Ypet-Ypet-expressing influenza viruses. 95

Figure 4.6. Virus replication kinetics in MDCK cells by plaque assay. 97

List of Tables

Table 2.1. Comparison of K_d from different methods 20

Table 2.2. K_d results of CyPetRanGap1c with YPetUbc9 under different conditions.. 35

Table 3.1. List of SUMOylation inhibitors by different groups 54

Table 4.1: Summary of results for SUMOylated lysine residues based on SUMOylation prediction tools 86

Table 4.2. Lysine residues mutated in each mutant YNS1 construct 89

List of Abbreviations

FRET: Förster resonance energy transfer

SUMO: small ubiquitin-like modifier

SENP: Sentrin/SUMO-specific protease

Uba: ubiquitin-like modifier activating enzyme

Ubc: ubiquitin-conjugating enzyme

PIAS: protein inhibitor of activated STAT

RanGAP: RanGTPase-activating protein

SPR: surface plasmon resonance

ITC: isothermal titration calorimetry

CFP/YFP: cyan/yellow fluorescent protein

SD: standard deviation

IC_{50}: half maximal inhibitory concentration

CHAPTER 1: INTRODUCTION

SUMOylation is an important mechanism for post-translational protein modification

Protein post-translational modification is a general mechanism that alters protein functions in eukaryotic cells. Common modification involves attachment of small chemical moiety such as phosphate, acetyl or methyl group, which plays a key role in many cellular events including signaling transduction, DNA repair and transcriptional regulation. Besides those small chemical moieties, small peptide can also function as protein modifier. Ubiquitin, a 76-residue peptide, is a well-studied protein modifier whose covalent modification can result in proteasome-mediated degradation of target proteins (1). *S*mall *U*biquitin-related *MO*difier, known as SUMO, has emerged as an important protein modifier in recent years. Composed of ~100 amino acids, SUMO undergoes reversible conjugation to the lysine residues of target proteins (SUMOylation) via the catalysis of various enzymes. Although structurally related to ubiquitin, SUMO only shares an 18% sequence identity with ubiquitin and has very different effects on target proteins (2). SUMOylation in a target-specific manner can affect a target protein's intracellular localization, its ability to interact with other proteins or its transcriptional activity (3). SUMOylation may also compete with ubiquitination on the same lysine residue to increase the stability of target proteins (4). Given its important role in many biological processes, SUMOylation is essential for most eukaryotic organisms. Although not well understood, there have been reports linking misregulated SUMOylation to many human diseases including carcinogenesis, neurodegenerative diseases and viral infection (5, 6).

SUMOylation is a cascade event involving multiple protein-protein interactions

Homologous to ubiquitination, conjugation and deconjugation of SUMO require the catalysis of multiple enzymes (Figure 1.1). SUMO is translated from mRNA as a precursor protein, Pre-SUMO. Pre-SUMO is then recognized by SUMO-specific peptidases (SENPs) and cleaved to generate a mature SUMO protein containing a C-terminal Gly-Gly motif. The heterodimer Aos1/Uba2, which composes the SUMO activating enzyme (E1), then forms a thioester bond with SUMO using the energy from the degradation of ATP. SUMO is further transferred from the E1 enzyme to the active cysteine residue of the SUMO E2 conjugating enzyme Ubc9. Catalyzed by SUMO E3 ligases, SUMO is finally transferred from Ubc9 to the lysine residue of target proteins. SUMOylated proteins can then be recognized by SENPs and bound SUMO is cleaved off to be reused for the conjugation to other proteins (3). Protein-protein interactions are crucial for SUMOylation to proceed. Using X-ray crystallography and protein-protein interaction assays such as yeast two-hybrid, interactions between different protein components have been investigated in the past few years. Co-crystallization of SUMO-E1 showed SUMO interacts with two distinct domains of heterodimer Aos1/Uba2 to form the thioester bond (7). Ubc9 possesses several protein interaction sites for E1, SUMO and E3 ligases and functions as the core component in the cascade (8, 9). SUMO E3 ligases interact with both substrate proteins and Ubc9/SUMO to facilitate transfer of SUMO by recruitment of substrate proteins.

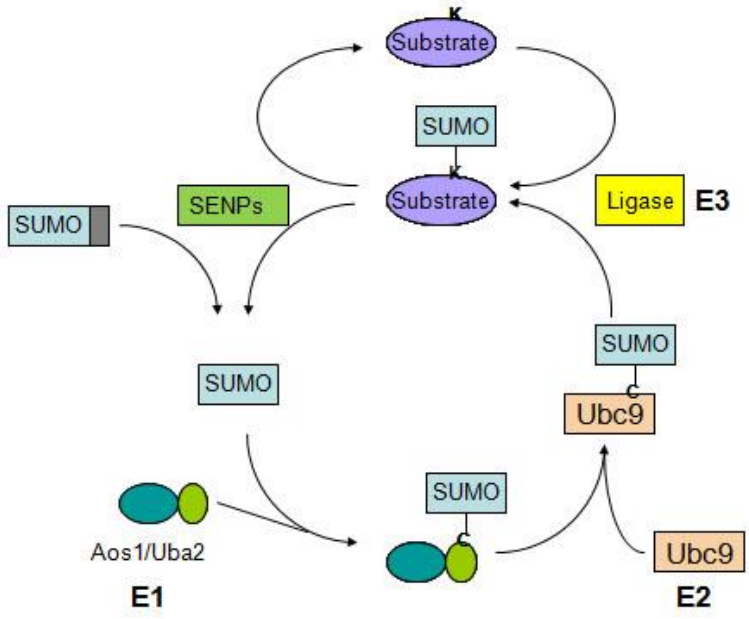

Figure 1.1. Conjugation and deconjugation of SUMO to and from substrate proteins require multiples enzymes.

As a three-enzyme cascade, SUMOylation involves many enzymes with different specificities. SUMO itself represents a family of closely related proteins. Four SUMO isoforms have been identified in human named as SUMO-1 to SUMO-4. Except SUMO-4 which is only expressed in the kidney and spleen, all SUMO proteins are ubiquitously expressed at all developmental stages (10). While SUMO isoforms share high sequence identity with each other (50% between SUMO-1 and SUMO-2, and 95% between SUMO-2 and SUMO-3), these isoforms are not functionally identical. Conjugation of SUMO2/3 but not SUMO-1 can be induced in response of certain stresses. Different SUMO isoforms are also used preferentially to modify different substrate proteins (3).

In contrast to E1 and E2 which have only one isoform each in human, E3 ligases are consisted of three distinct types of proteins: the PIAS [protein inhibitor of activated STAT (signal transducer and activator of transcription)] family, the polycomb group protein Pc2 and the nuclear pore complex protein RanBP2. Among the three types of E3 ligases, PIAS proteins have been most extensively studied. Human genome encodes four PIAS genes, PIAS1, PIAS3, PIASx and PIASy. PIAS proteins share a high sequence homology. They all feature a SP-RING domain, which is crucial for binding Ubc9, and a SUMO interaction motif (SIM) implicated in directly binding SUMOs (11). PIAS proteins were first identified by their ability to interact with and inhibit the transcriptional activity of STAT proteins (12). PIAS1 and PIAS3 interact with STAT1 and STAT3 respectively with high specificity (12, 13). Later it was discovered that PIAS proteins can also function as SUMO E3 ligases to induce SUMOylation of the proteins they interact with (13). In the case of cytokine signaling pathways, binding of interferon gamma to its receptor leads to

activation of STAT1, which translocates into nucleus and induces downstream gene expression. PIAS1 interacts with activated STAT1 and induces SUMOylation of STAT1 to inhibit its transcriptional activity, therefore ensuring proper regulation of interferon signaling (14) (Figure 1.2). Besides STAT proteins, PIASs can also promote SUMOylation of a variety of structurally diverse proteins. Most of these proteins are transcriptional factors including p53, whose transcriptional activity is strongly repressed by PIAS1-mediated SUMOylation (15).

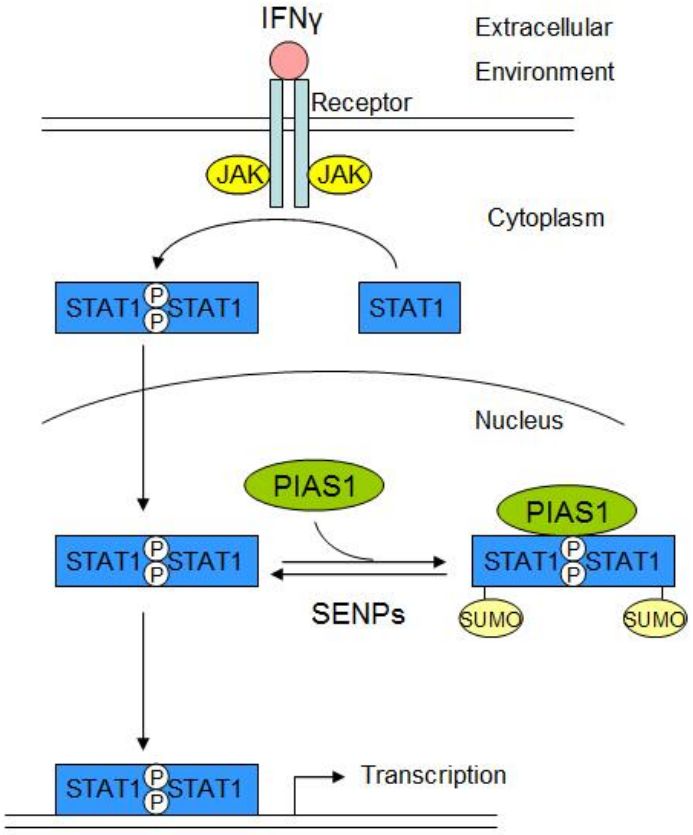

Figure 1.2. Inhibition of STAT1-mediated IFNγ pathway by PIAS1, a SUMO E3 ligase.

Small chemical compounds can serve as useful tools to study the SUMOylation network

While SUMOylation plays an important role in many biological processes including regulation of immune signal transduction, stabilization of target proteins and maintenance of chromosomal integrity, the investigation of SUMOylation network *in vivo* has been hindered by many challenges. Conjugation and deconjugation of SUMO are highly dynamic processes and SUMO can be quickly removed upon cell lysis unless cells are lysed in denaturing conditions or protease inhibitors are added (3). Furthermore, given the important roles they play, gene knockout of components in SUMOylation can be lethal. Depletion of SUMO1 or the E2 enzyme in mice is embryonically lethal (16, 17). PIAS1 deficient mice are partially embryonically lethal and the activity of their interferon-mediated JAK-STAT pathway is deregulated (18). To overcome these difficulties, new tools besides the traditional biochemical and genetic approaches are needed to study the SUMOylation network.

Among a variety of techniques for biological research, small chemical compounds stand as unique tools to manipulate the activity of biological processes. Compared with other biological approaches, bioactive small chemical compounds not only offer better spatial and temporal control of biological processes but also can be used to investigate the biological function of proteins when gene knockout studies are not feasible. While most chemical compounds used in biological research are receptor agonists/antagonists or enzyme inhibitors, small chemical compounds disrupting non-enzyme protein-protein interactions have emerged as useful tools. Nutlin-3, an ubiquitin E3 ligase inhibitor

developed in 2004, has been shown to induce apoptosis and growth inhibition of cancer cells by disrupting the interaction of ubiquitin E3 ligase MDM2 and its substrate p53 (19). Homologous to ubiquitination, SUMOylation requires interactions between SUMO, catalyzing enzymes and substrate proteins. Therefore, small chemical compounds disrupting interactions between components in SUMOylation will be very useful to dissect the whole network. A recently found small compound SUMOylation inhibitor-STE through FRET-based high-throughput screening assay has been proven to specifically bind to SUMO E1. Research on the mechanism of STE inhibition of the SUMO E1 will help us understand how SUMOylation regulates the transcriptional program for tumorigenesis and cytokine pathway for innate immunity.

FRET-based technique is a powerful tool for studying protein-protein interaction

FRET occurs between two adjacent fluorophores when their distance is smaller than 1-10nm and the emission spectrum of donor has more than 30% overlapping with the excitation spectrum of acceptor. Energy transferred from excited donor to acceptor results in quenching of donor and excitation of acceptor (Figure 1.3). Because the efficiency of energy transfer is highly dependent (sixth-power) on the distance between donor and acceptor fluorophores, FRET-based techniques have been extensively used in biological research including identification of protein interactions, real-time monitoring of intracellular signaling activities, and high-throughput screening of bioactive molecules (20-22). Compared with traditional techniques used to identify protein-protein interactions such as co-immunoprecipitation and yeast two-hybrid, FRET can offer real-time monitoring in living cells and is easier to be adapted into high-throughput screening. In

FRET-based assays, proteins are tagged with different fluorophores to form FRET pairs. Interaction of proteins recruits fluorophores together and increase the efficiency of energy transfer from donor fluorophores to acceptor fluorophores. Disruption of protein-protein interactions by small chemical inhibitors will separate the fluorophores apart and result in decreased FRET signal of the system.

Traditionally, FRET-based assays utilize organic fluorophores to modify proteins of interest, which strongly limits its application in protein assays. Our *in vitro* assays, which utilize fluorescently fused recombinant proteins, are easier to handle but fail to completely emulate the native environment of the target proteins in living cells. Fluorescent proteins have been most extensively used to label proteins *in vivo* due to the ease of genetic labeling. An engineered FRET pair, CyPet and YPet, were used in this research. CyPet and YPet are developed from CFP and YFP with much higher fluorescence quantum yield and FRET efficiency (23). Various efforts have been made to develop qFRET methods to accurately determine the interaction affinity and kinetics parameters [24,25].

(A)

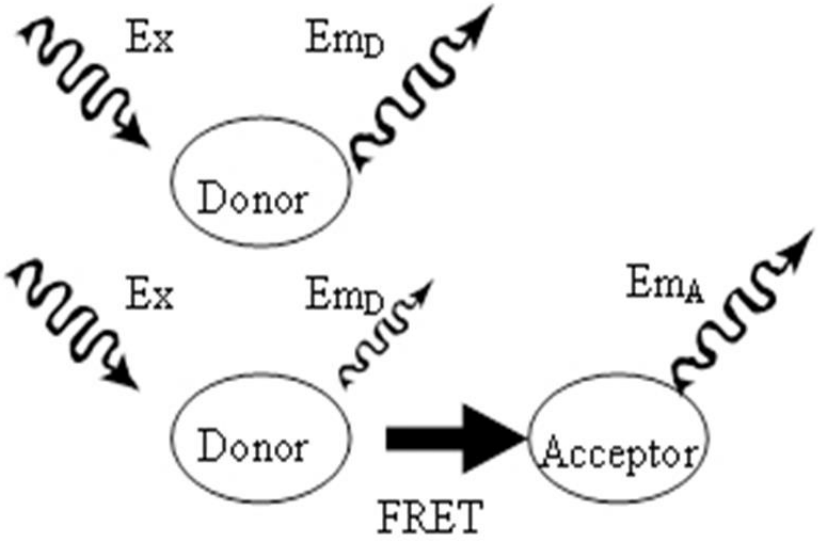

(B)

$$E = \frac{1}{1 + (r/R_0)^6}$$

Figure 1.3. Principal of FRET. (A) Principle of FRET. (B) FRET efficiency E is dependent on the distance r between the donor and acceptor to the power of six.

Regulation of cytokine signaling pathways by PIAS proteins and SUMO conjugation

Cytokines are small polypeptides or glycoproteins secreted by a variety of cells to modulate cell growth and differentiation. Many cytokines are found to play important roles in regulating immune and inflammatory responses. Cytokines bind to their cell surface receptors to activate multiple signal transduction pathways to regulate gene expression. The distinct biological functions of cytokines largely result from the differential gene expression patterns triggered by cytokines. Signal transducer and activator of transcription proteins (STATs) and nuclear factor-kappaB (NF-kappaB) are two key families of transcription factors that are widely used by cytokines to modulate gene expression. Upon cytokine stimulation, STATs and NF-kappaB become activated in the cytoplasm, and then translocate into the nucleus where they activate transcription. These cytokine-mediated gene activation pathways are tightly controlled by both positive and negative regulators. Abnormal cytokine signaling is associated with cancer and immune disorders.

Biochemical and genetic studies have discovered a critical role of the PIAS (protein inhibitor of activated STAT) protein family in the regulation of cytokine signaling. Several molecular mechanisms have been proposed to explain how PIAS proteins might regulate transcription. In case of regulation of IFNγ signaling pathway, PIAS may inhibit transcription by blocking the DNA-binding activity of a transcription factor or regulate transcription by promoting the SUMOylation of a transcription factor [26]. Recent research showed that phosphorylation of STAT1 at Tyr701 and SUMOylation at the adjacent Lys703 are mutually exclusive, but the physiological significance of STAT1 SUMOylation has not been fully explored [27].

CHAPTER 2: Determine Protein Interaction Affinity Without Protein Purification by Quantitative FRET (qFRET) Technology

Abstract

Protein interactions are fundamental for many processes in cellular lifecycles. The dissociation constant, K_d, is generally used to determine protein-protein interaction affinity. The traditional methods for K_d determinations, such as surface plasmon resonance (SPR), isothermal titration calorimetry (ITC), radioactive labeling and ultracentrifugation have been widely used to determine protein interaction affinity. However, these techniques normally require purified proteins for determining protein interaction affinity. In this chapter I will describe a novel development for determining protein dissociation constant directly from bacterial extract without protein purification using qFRET technology. We applied this methodology to determine the interaction affinity between SUMO E2-Ubc9 and its substrate, RanGap1c. SUMOylation, a multi-step enzymatic cascade to modify proteins *in vivo*, has been shown to be involved in various physiological and pathological processes. The method of qFRET has been developed for the systematic determination of protein interaction dissociation constant K_d between Ubc9 and RanGap1c in the presence of BSA or *E. coli* lysates, or both proteins in a mixture of bacterial extract. The K_d (~0.10 μM) are consistent in various assay conditions and comparable to the value from SPR measurement. The results demonstrate generality of qFRET-based K_d determination methodology. Therefore, this technique has a great advantage over traditional approaches

for determining protein interaction affinity in the presence of multiple contaminant proteins, and can be potentially translated into a high-throughput assay.

Introduction

Protein-protein interactions play critical roles in many physiological processes. One of the most commonly used biochemical parameters to define the affinity of protein-protein interactions a is the dissociation constant (24). The traditional methods for measuring K_d are surface plasma resonance (SPR) (25, 26), isothermal titration calorimetry (ITC) (27, 28), and radioactive ligand binding assay (29). These methods serve as standard approaches for determining binding affinity parameters, in which the quantifications of K_d values are proven to be accurate and reliable. However, these techniques usually require expensive instrumentation, tedious procedures and special reagents (e.g. radioactive labels in radioactive ligand binding assay). More importantly, most traditional methods require multi-step protein purification process for protein labelling or conjugation to determine protein interaction affinities, which is seldom applied on proteins with low expression yield and/or low purity but with high research interest, such as protein inhibitor of activated STAT (PIAS) or G-protein-coupled receptors (GPCRs).

SUMOylation is one of the most important post-translational modification, which serves as a key mechanism that regulates protein activities and stability in a variety of physiological processes. SUMO proteins, like ubiquitin (Ub) or other ubiquitin-like proteins (Ubls), are conjugated to the target proteins in an evolutionarily conserved three-step enzymatic cascade which involves the sequential actions of E1-acitvation enzyme, E2-conjugation enzyme and E3 ligase (3). The whole SUMOylation pathway starts from maturation of SUMO in which the precursor protein pre-SUMO is recognized and cleaved at its C-terminal by SUMO-specific protease (SENPs) to expose the C-terminal Gly-Gly

motif (3, 30). SUMO is then activated through adenylation by the Aos1 subunit of SUMO E1 enzyme, and transferred to Uba2 subunit to form the SUMO-E1 complex with the formation of thioester bond between the C-terminal glycine of SUMO and cysteine residue of Uba2 (31). This is followed by SUMO being further transferred to SUMO E2 enzyme Ubc9 with a formation of a thioester bond to the cysteine active residue of Ubc9. Then SUMO E3 ligases can catalyze the final transfer of SUMO to the lysine residue of target substrates. Although, SUMO E1 and E2 enzymes are sufficient for SUMOylation to occur without E3 activity in most situations *in vitro*, many studies showed that E3 ligase functions as an adaptor that recruits and stabilizes the binding of SUMO-E2 complex with target proteins and promote SUMOylation (32, 33). The specificity of SUMOylation on different acceptor proteins is proposed to be controlled by SUMO E3 activity (3, 34). Since each step of the sequential SUMO-transferring cascade reactions involves protein interactions between the key SUMOylation components, quantitative and systematic studies of these protein interactions will elucidate the details of the cascade mechanism.

Förster resonance energy transfer (FRET) has been widely used as a quantitative method for determining molecular interactions within a distance of 10 nm. Since the FRET signal is highly dependent on the molecular distance of donor and acceptor, FRET-based assays have been developed into a sensitive and effective tool for deciphering molecular interactive events (35). Martin was the first to establish a FRET-based assay to quantify the protein interaction dissociation constant K_d (36). In his study, a commonly used FRET-pair, CFP and YFP were tagged on the target proteins, SUMO1 and Ubc9 respectively, for determination of interaction affinity between the two core SUMOylation components.

When fixed concentrations of CFP-SUMO1 and increasing concentrations of YFP-Ubc9 were mixed in the system, the steady-state binding of SUMO1 and Ubc9 was observed with FRET. To subtract the contaminate FRET portion from the direct emission of the acceptor, an external standard curve was established to calculate the fluorescence spectrum from mixture of CFP and YFP-Ubc9. With the assumption that the absolute FRET intensity is linearly proportional to the bound concentration of YFP-Ubc9, the free and bound YFP-Ubc9 concentrations were derived from the measurement and fit in a hyperbolic equation to calculate K_d. The major disadvantage of this approach is that the external standard curve requires additional experiments which use different fluorescent proteins from those used in K_d measurement, which could cause significant experimental errors.

To solve the major challenge of spectrum crosstalk between the FRET donor and acceptor, our group has previously developed a method which uses internal standard curve to calculate the emission spectrum overlap between donor and acceptor (37). A novel FRET pair, CyPet and YPet with greater FRET efficiencies which were engineered from CFP and YFP, respectively, in 2005 was used in this method (23). The peak excitation/emission wavelengths of CyPet and YPet are 414 nm/475 nm and 515 nm/530 nm, respectively. CyPet and YPet were fused to the N-terminus of SUMO1 and Ubc9 respectively through gene cloning method. When CyPet-SUMO1 and YPet-Ubc9 were mixed, the excitation of CyPet at 414 nm would cause quenching of CyPet emission at 475 nm and increase of YPet emission at 530 nm due to the binding of SUMO1 and Ubc9. Since the observed FRET signal also consists of direct emissions from donor and acceptor at excitation/emission wavelengths of 414 nm/530 nm, these crosstalk contributions need

to be eliminated from total FRET emission before further analysis. An internal cross-wavelength co-efficiency method was established for the qFRET signal analysis. In this analysis, the direct emission at 530 nm was dissected into three components: the direct emission of CyPet, the direct emission of YPet and the emission of YPet from energy transfer of donor (Figure 2.1A). In the FRET assay, the mixture of CyPet-SUMO1 and YPet-Ubc9 was excited at 414 nm, and two emission signals at 475 nm (FL_{DD}) and 530 nm (FL_{DA}) were determined (Figure 2.1A), respectively. A second excitation at 475 nm was used to determine the fluorescence emission of YPet-Ubc9 (FL_{AA}) by itself (Figure 2.1B). Two specific cross-wavelength ratios were then calculated to determine the direct emission portions from total FRET signal (FL_{DA}): the α ratio for CyPet with excitation/emission wavelengths set at 414 nm/530 nm and 414 nm/475 nm (Figure 2.1C), and the β ratio for YPet with excitation/emission wavelengths set at 414 nm/530 nm and 475 nm/530 nm (Figure 2.1D). Since the two wavelength coefficient ratios remain constant for a specific FRET pair, they can be easily determined before mixing. With these factors defined, the direct emission components of CyPet and YPet can be calculated and subtracted from total FRET emission (Figure 2.1E) (38).

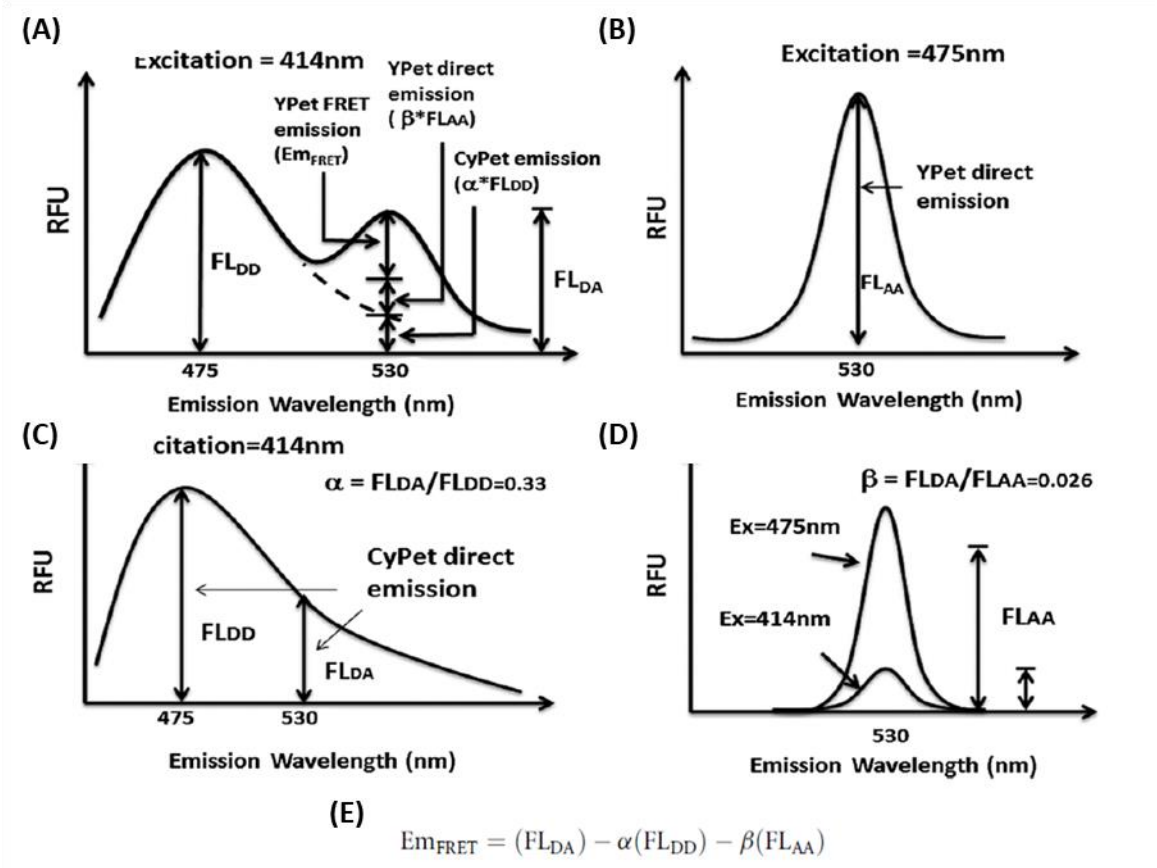

Figure 2.1. Quantitative spectrum analysis of FRET signal. (A) Total FRET signal at acceptor emission wavelength when excited at donor excitation wavelength (FL_{DA}) consists of three components: absolute FRET emission from YPet, direct emission of donor, CyPet, and direct emission of acceptor, YPet. (B) Acceptor emission when excited at acceptor excitation wavelength (FL_{AA}). (C) Donor emission at donor emission wavelength (FL_{DD}) which is proportional to its contribution for total FRET signal. (D) FL_{AA} is proportional to acceptor's contribution for total FRET signal. (E) Determination of absolute FRET (Em_{FRET}) from total FRET signal.

The absolute FRET signal (Em_{FRET}) is linearly proportional to the bound concentration of YPet-Ubc9, which can also be expressed as a function of K_d and total concentration of YPet-Ubc9 in the assay by definition, thus a mathematical formula as shown below was derived to correlate K_d with Em_{FRET} to quantitatively derive the K_d of target proteins interaction affinity (37).

$$Em_{FRET} = Em_{FRETmax}\left(1 - \frac{2K_d}{X - a + K_d + \sqrt{(X - a - K_d)^2 + 4K_dX}}\right)$$

Here, X represents total concentration of YPet-Ubc9 at each titration point, a represents total concentration of CyPet-SUMO1 which is constant in the assay, and $Em_{FRETmax}$ represents the theoretical maximal value of Em_{FRET} when 100% YPet-Ubc9 in the assay is bound to CyPet-SUMO1. The data of Em_{FRET} at each YPet-Ubc9 concentration point is fitted into this formula to derive the best-fit value of K_d. This method produces K_d results comparable with those from SPR or ITC assays (Table 2.1) (39). However, this approach is applied on purified CyPet-SUMO1 and YPet-Ubc9, and it usually requires several micromoles of proteins for the assay, which can hardly be achieved for some proteins with low yield and/or low purity due to their toxicity in host cells, insolubility or their roles as membrane proteins. PIAS proteins- which are a major family of SUMO E3 ligases and found to be associated with several cancers- are poorly expressed from the commonly used *E. coli* expression system. The study of the binding affinities of PIAS with other SUMOylation proteins, which has not been reported before, can elucidate the mechanism of how PIAS regulates SUMOylation of different target proteins under the corresponding physiological or pathological conditions.

Table 2.1. Comparison of K_d from different methods

Methods	Protein pairs	K_d (mmol/L)
FRET	CyPet-SUMO1+YPet-Ubc9	0.30±0.03
SPR	CyPet-SUMO1+YPet-Ubc9	0.35
SPR	SUMO1+Ubc9	0.10
ITC	SUMO1+Ubc9	0.25±0.07

In principal, FRET signal is only dependent on physical natures and bound percentage of target interactive proteins, regardless of the presence and interactions of other contaminate proteins in the system. In this chapter, I will describe how we expand the qFRET-based K_d measurement to a broad range of assay conditions, including addition of BSA or *E. coli* lysates, and furthermore this method can be used to determine protein interaction affinity directly from bacterial crude extract without purification. The systematic K_d determination of Ubc9 with SUMOylation substrate RanGap1c shows that the values of K_d (~0.10 μM) are consistent in various assay conditions and comparable to the value from SPR measurement.

Materials and Methods

DNA constructs

The open reading frames of CyPet and YPet were amplified by PCR with primers containing NheI-SalI sites. The sizes of PCR products were 729 and 729 bp, respectively. RanGAP1c and Ubc9 were amplified by PCR with primers containing SalI-NotI sites. All these four genes were cloned into pCRII-TOPO vector (Invitrogen). Then the fragments encoding RanGAP1c and Ubc9 were extracted after digestion by SalI and NotI and inserted into pCRII-CyPet or pCRII-YPet linearized by SalI and NotI. After the sequences were confirmed, the cDNAs encoding CyPetRanGAP1c and YPetUbc9 were cloned in between the NheI-NotI sites of pET28(b) vector (Novagen).

Protein expression and purification

BL21(DE3) *Escherichia coli* cells were transformed with pET28(b) plasmids encoding CyPetRanGAP1c or YPetUbc9. The transformed bacteria were plated on LB agar plates containing 50 μg/mL kanamycin, and single colonies were picked up and expanded in 2xYT medium to optical density of 0.5–0.8 at 600 nm. The expression of polyhistidine-tagged recombinant proteins was induced with 0.3 mM isopropyl β-D-thiogalactoside. Bacterial cells were collected by centrifugation at 6,000 rpm for 10 min, then resuspended in binding buffer (20 mM Tris-HCl, pH 7.4, 500 mM NaCl and 5 mM imidazole), and lysed by sonication using ultrasonic liquid processor (Misonix). Cell lysates containing recombinant proteins were cleared by centrifugation at 35,000 g for 30 min. The polyhistidine-tagged recombinant proteins were then purified from bacterial lysates by Ni^{2+}-NTA purification system (QIAGEN). The beads-bound proteins were washed by three

different washing buffers in sequence (Washing buffer 1 contained 20 mM Tris-HCl, pH 7.4, 300 mM NaCl. Washing buffer 2 contained 20 mM Tris-HCl, pH 7.4, 1.5 M NaCl, and 5% Triton X-100. Washing buffer 3 contained 20 mM Tris-HCl, pH 7.4, 500 mM NaCl, and 20 mM imidazole), and eluted by elution buffer (20 mM Tris-HCl, pH 7.4, 200 mM NaCl, and 250 mM imidazole). Then the proteins were dialyzed in dialysis buffer (20 mM Tris-HCl, pH 7.4, 50 mM NaCl, and 1 mM DTT) overnight. The purity of proteins was examined by SDS-PAGE gel with Coomassie blue staining, and protein concentrations were determined using Coomassie Plus Protein Assay (Thermo Scientific).

FRET measurement

Four groups of K_d measurement on CyPetRanGAP1c and YPetUbc9 with different assay conditions were conduct. Firstly, purified CyPetRanGAP1c and YPetUbc9 proteins were mixed at room temperature in Tris buffer (20 mM Tris-HCl, pH 7.5, 50 mM NaCl, DTT 1 mM) to total volume of 60 µL. The final concentrations of CyPetRanGAP1c were fixed to 0.05, 0.1, 0.5 or 1.0 µM and the final concentrations of YPetUbc9 were varied from 0 to 4 µM. Secondly, 1, 3 or 10 µg blank BL21 bacterial extract was added to all samples with same concentration combinations of CyPetRanGAP1c and YPetUbc9 as described above. Thirdly, 1 µg pure BSA was added to all samples with same concentration combinations of CyPetRanGAP1c and YPetUbc9. And lastly, unpurified CyPetRanGAP1c and YPetUbc9 from crude BL21 bacterial extract were mixed at the same concentration combinations as above. Molar concentrations of unpurified CyPetRanGAP1c and YPetUbc9 were calculated from fluorescence standard curve. The three-wavelength fluorescence signals were measured from all samples of each group using

fluorescence multi-well plate reader FlexstationII384 (Molecular Devices, Sunnyvale, CA). Specifically, fluorescence emission signals at 475 and 530 nm were measured under excitation wavelength at 414 nm with cutoff filter set at 455 nm. Fluorescence emission signal at 530 nm was measured at the excitation wavelength at 475 nm with a cutoff filter set at 515 nm. Each sample was prepared in triplicate, and the fluorescence signals were averaged before further data processing.

Standard curves for CyPetRanGAP1c and YPetUbc9

Different concentrations of purified CyPetRanGAP1c or YPetUbc9 were incubated at 37ºC for five minutes in Tris buffer (20 mM Tris-HCl, pH 7.4, 50 mM NaCl, DTT 1 mM) at total volume of 60 μL and distributed to each well of 384-well black/clear plate. The fluorescence signals at Ex 414 nm/ Em 475 nm and Ex 475 nm/ Em 530 nm were measured respectively on CyPetRanGAP1c and YPetUbc9 varying from 0 to 2 μM to establish the standard curves for CyPetRanGAP1c and YPetUbc9.

Spectrum analysis of FRET

When the mixture of CyPetRanGAP1c and YPetUbc9 recombinant proteins was excited at 414 nm, the observed emission intensity at 530 nm consisted of three components: direct contribution from CyPetRanGAP1c which is proportional to the donor emission signal at Ex 414 nm/ Em 475 nm (FL_{DD}) with a ratio factor of α, sensitized emission of YPetUbc9 (Em_{FRET}) and direct contribution from YPetUbc9 which is proportional to the acceptor emission signal at Ex 475 nm/ Em 530 nm (FL_{AA}) with a ratio factor of β. And only Em_{FRET} is proportional to the amount of bound YPetUbc9.

To determine the ratio constant of α, a series of CyPetRanGAP1c were prepared at concentrations of 0.05, 0.1, 0.5, 1.0 μM. The emissions of CyPetRanGAP1c at 475 (FL_{DD}) and 530 nm (FL_{DA}) were measured when excited at 414 nm. The average ratio constant α was calculated from the ratio of FL_{DD} to FL_{DA}. To determine the ratio constant of β, a series of YPetUbc9 were prepared at concentrations of 0.2, 0.5, 1, 2, 3, and 4 μM. The emissions of YPetUbc9 at 530 nm were measured when excited at 414 (FL_{DA}) and 475 nm (FL_{AA}). The average ratio constant β was calculated from the ratio of FL_{AA} to FL_{DA}.

Data processing and K_d determination

After Em_{FRET} at each specific condition was calculated as described above, the datasets of Em_{FRET} versus total concentration of YPetUbc9 ($[YPetUbc9]_{total}$) were fit to the equation shown below by Prism 5 (GraphPad Software) to derive the best-fit values for $Em_{FRETmax}$ and K_d. Specifically, the values of $[YPetUbc9]_{total}$ were put into X-column, and the values of Em_{FRET} in triplicate at each $[YPetUbc9]_{total}$ were put into Y-column. Nonlinear regression was used to fit the datasets:

$$Y=Em_{FRETmax}-2*Em_{FRETmax}*K_d/(X-A+K_d+sqrt(sqr(X-A-K_d)+4*K_d*X))$$

Initial values of parameters $Em_{FRETmax}$ and K_d were set to 1.0. $Em_{FRETmax}$ value was constrained to be greater than 0. A was set to be a constant equal to 0.05, 0.1, 0.5 or 1.0 μM based on the total concentration of CyPetRanGAP1c. The results were reported as mean ± SD.

K_d determination of non-covalent RanGAP1c and Ubc9 interaction by SPR

His-tagged YPetUbc9, CyPetRanGAP1c, Ubc9 and RanGAP1c were dialyzed overnight in running buffer (10 mM HEPES, 150 mM NaCl, 50 μM EDTA, 0.005%

Tween20 pH7.4). The analysis of interaction between CyPetRanGAP1c and YPetUbc9 or RanGAP1c and Ubc9 was performed on BIAcore X100 system equipped with NTA sensor chips (BIAcore AB, Uppsala, Sweden) at a flow rate of 30 µL/min. For immobilization of proteins, the chip was treated with 500 µM $NiCl_2$ in running buffer for 1 min, and then 100 ng/mL purified YPetUbc9 or 200 ng/mL purified Ubc9 was injected for 120 s and stabilized for 120 s. Then 50~160 µg/mL thrombin-digested CyPetRanGAP1c or 10~40 µg/mL thrombin-digested RanGAP1c was injected for 120 s and disassociated for 10 min. To continuously monitor the nonspecific binding of samples to the NTA surface, CyPetRanGAP1c or RanGAP1c protein was injected into a control flow cell without treatment of $NiCl_2$ and YPetUbc9/Ubc9 protein. After each set of experiment with one concentration of CyPetRanGAP1c or RanGAP1c, NTA sensor chip was regenerated by regeneration buffer (10 mM HEPES, 150 mM NaCl, 350 mM EDTA, 0.005% Tween20 pH8.3), then retreated by $NiCl_2$, and immobilized by YPetUbc9 or Ubc9 for the next set of experiment with a different concentration of CyPetRanGAP1c or RanGAP1c. All measurements were performed at 25^{o}C in running buffer. Data was analyzed with BIAcore X100 evaluation software ver.1.0 (BIAcore).

Results

Design of qFRET-based approach for K_d determination of Ubc9-RanGAP1c interaction in the presence of other proteins

QFRET-based approach was used to measure Em_{FRET} which is correlated to dissociation constant K_d of RanGAP1c and Ubc9 under different conditions. For each condition in the absence or presence of other proteins, fixed concentration of CyPetRanGAP1c and titrated concentration of YPetUbc9 384 were mixed in 384-well black/clear plate, and three-wavelength measurement was performed to calculate Em_{FRET}. Ideally, the bound RanGAP1c and Ubc9 will bring CyPet and YPet in close proximity which results in fluorescence resonance energy transfer. And the absolute FRET signal is proportional to the amount of bound RanGAP1c and Ubc9, regardless of other contaminate proteins in the assay (Figure 2.2A).

In this assay, the binding of RanGAP1c and Ubc9 can be analyzed by coupling Em_{FRET} signal with concentration of bound YPetUbc9. Firstly, the dissociation constant, K_d, can be defined as: (Figure 2.2B)

$$K_d = \frac{[\mathrm{CyPetRanGAP1c}]_{\mathrm{free}}[\mathrm{YPetUbc9}]_{\mathrm{free}}}{[\mathrm{CyPetRanGAP1c{\cdot}YPetUbc9}]} = \frac{[\mathrm{CyPetRanGAP1c}]_{\mathrm{free}}[\mathrm{YPetUbc9}]_{\mathrm{free}}}{[\mathrm{YPetUbc9}]_{\mathrm{bound}}},$$

This can be rearranged to

$$[\mathrm{YPetUbc9}]_{\mathrm{bound}} = \frac{[\mathrm{YPetUbc9}]_{\mathrm{bound\ max}}[\mathrm{YPetUbc9}]_{\mathrm{free}}}{\mathrm{K_d}+[\mathrm{YPetUbc9}]_{\mathrm{free}}} \quad (1)$$

Where $[YPetUbc9]_{boundmax}$ is the theoretical maximal YPetUbc9 concentration bound to CyPetRanGAP1c, and $[YPetUbc9]_{free}$ is the free YPetUbc9 concentration. Since$[\mathrm{YPetUbc9}]_{\mathrm{bound}}$ is proportional to $Em_{FRET:}$

$[YPetUbc9]_{bound}/[YPetUbc9]_{bound\ max}=Em_{FRET}/Em_{FRETmax}$

Eq (1) can be converted into Eq (2)

$$Em_{FRET} = Em_{FRET\,max}\left(1 - \frac{2K_d}{X-A+K_d+\sqrt{(X-A-K_d)^2+4K_dX}}\right) \quad (2)$$

Where Em_{FRET} is the absolute FRET signal and $Em_{FRETmax}$ is the absolute FRET signal at maximal concentration of bound YPetUbc9. A is the total concentration of CyPetRanGAP1c ($[CyPetRanGAP1c]_{total}$). X is the total concentration of YPetUbc9 ($[YPetUbc9]_{total}$).

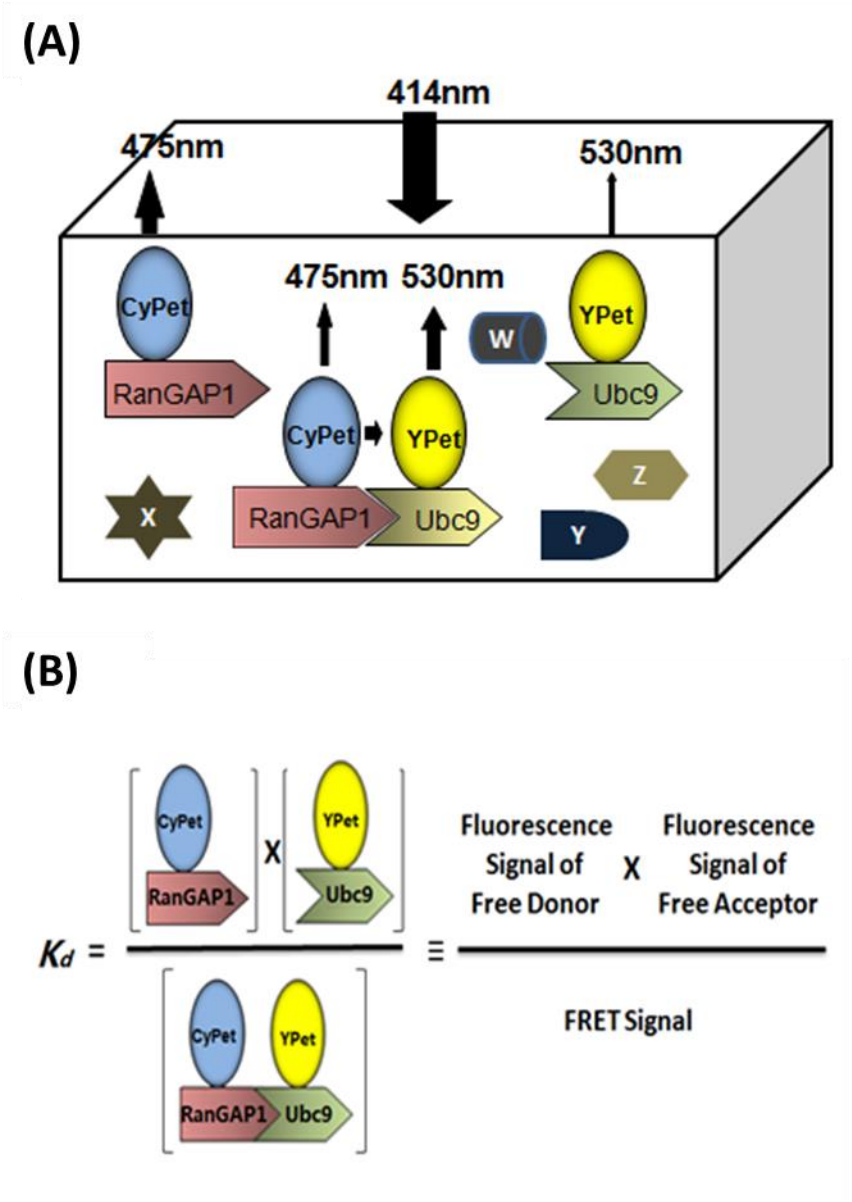

Figure 2.2. Schematic diagram of FRET-based assay for determination of protein interaction dissociation constant, K_d, in the presence of other proteins. (A) Schematic graph of fluorescence excitation and emission signals of interactive proteins, CyPetRanGAP1c and YPetUbc9, in the presence of other proteins. (B) The formula of K_d determination by FRET and fluorescence signals.

FRET-based assay for K_d determination

To obtain the absolute FRET signal (Em_{FRET}) for K_d measurement, the direct emissions at 530 nm from donor (CyPet) and acceptor (YPet) need to be determined and excluded from the total emission at 530 nm. The direct emission of unquenched donor CyPet at 530 nm is proportional to its emission at 475 nm when excited at 414 nm with a ratio factor of α ($\boldsymbol{\alpha}$***FL**$_{DD}$, FL_{DD} is the fluorescence emission of CyPet at 475 nm when excited at 414 nm), while the direct emission of YPet at 530 nm is proportional to its emission at 530 nm when excited at 475 nm with a ratio factor of β ($\boldsymbol{\beta}$*FL_{AA}, FL_{AA} is the fluorescence emission of YPet at 530 nm when excited at 475 nm) (Figure 2.3B). Therefore, the absolute FRET signal (Em_{FRET}) can be determined as:

$$Em_{FRET} = FL_{DA} - \alpha * FL_{DD} - \beta * FL_{AA}$$

where the ratio constants α and β were experimentally determined as 0.334±0.003 and 0.014±0.002, using free CyPetRanGAP1c and YPetUbc9, respectively.

In our previous studies, we analyzed the protein interaction affinity of CyPet-SUMO1 and YPetUbc9 by qFRET assay. The FRET-based K_d measurement provides reliable K_d values and has several advantages over other standard methods for K_d measurement, such as a radiolabeled ligand binding assay, SPR or isothermal titration calorimetry. The SUMO substrate and E2, RanGAP1c and Ubc9 are important in the SUMOylation pathway. Also, the SUMOylation pathway occurs without E3 *in vitro*. Thus, the interaction affinity between RanGAP1c and Ubc9 can help understand the thermodynamics of E2-mediated substrate SUMOylation.

We first tested the sensitivity of FRET assay at different concentrations of CyPetRanGAP1c. Figure 2.3A shows the spectra (Ex=414 nm) from one set of experiment, in which the CyPetRanGAP1c concentration was fixed to 1 μM. As the concentration of YPetUbc9 gradually increased from 0 to 4 μM, the binding of YPetUbc9 to CyPetRanGAP1c which resulted in energy transfer from CyPet to YPet caused significant increase of FRET emission at 530 nm, while the direct emission at 475 nm from unquenched CyPetRanGAP1c decreased. We then measured the fluorescence emissions of each group at four different concentrations of CyPetRanGAP1c. In each set of experiment, the concentration of CyPetRanGAP1c was fixed to 0.05, 0.1, 0.5 or 1.0 μM, and the concentration of YPetUbc9 increased from 0 to 4 μM. The fluorescence emission intensities of all samples were monitored at three-wavelength setting to exclude the direct emissions of CyPetRanGAP1c and YPetUbc9 from total FRET signal. After subtracting the direct emissions of CyPetRanGAP1c and YPetUbc9, the absolute FRET emission (at 530 nm when Ex=414 nm) was found to increase steadily as higher concentration of YPetUbc9 was used at each concentration of CyPetRanGAP1c (Figure 2.3A).

To determine $Em_{FRETmax}$ and K_d, we fit the data from each set of experiment with different total concentration of CyPetRanGAP1c in Equation (2) using nonlinear regression. The best-fit values for $Em_{FRETmax,}$ were $(1.227\pm0.022)\times10^4$, $(2.433\pm0.041)\times10^4$, $(12.29\pm0.23)\times10^4$, and $(24.61\pm0.53)\times10^4$, for 0.05, 0.1, 0.5 and 1.0 μM of CyPetRanGAP1c, respectively. In this concentration range of the binding partner, the $Em_{FRETmax}$ had a linear relationship with amount of CyPetRanGAP1c from 3 to 60 pmole (R^2= 1.000, Figure 2.6A and

Table 2.2). This result suggests that our approach can accurately and consistently predicts $Em_{FRETmax}$ at various concentration ratios of CyPetRanGAP1c to YPetUbc9.

The values of K_d for different concentrations of CyPetRanGAP1c (0.05, 0.1, 0.5, and 1.0 μM) used in the assay, are 0.098±0.014, 0.096±0.013, 0.101±0.016, and 0.114±0.021 μM, respectively (Table 2.2). The very consistent K_ds generated from different concentrations of CyPetRanGAP1c(0.05, 0.1, 0.5, and 1.0 μM) and a wide range of binding partner ratios of CyPetRanGAP1c to YPetUbc9 (from 0.67 to 40 folds) also demonstrate that FRET-based K_d measurement approach is very robust and reliable.

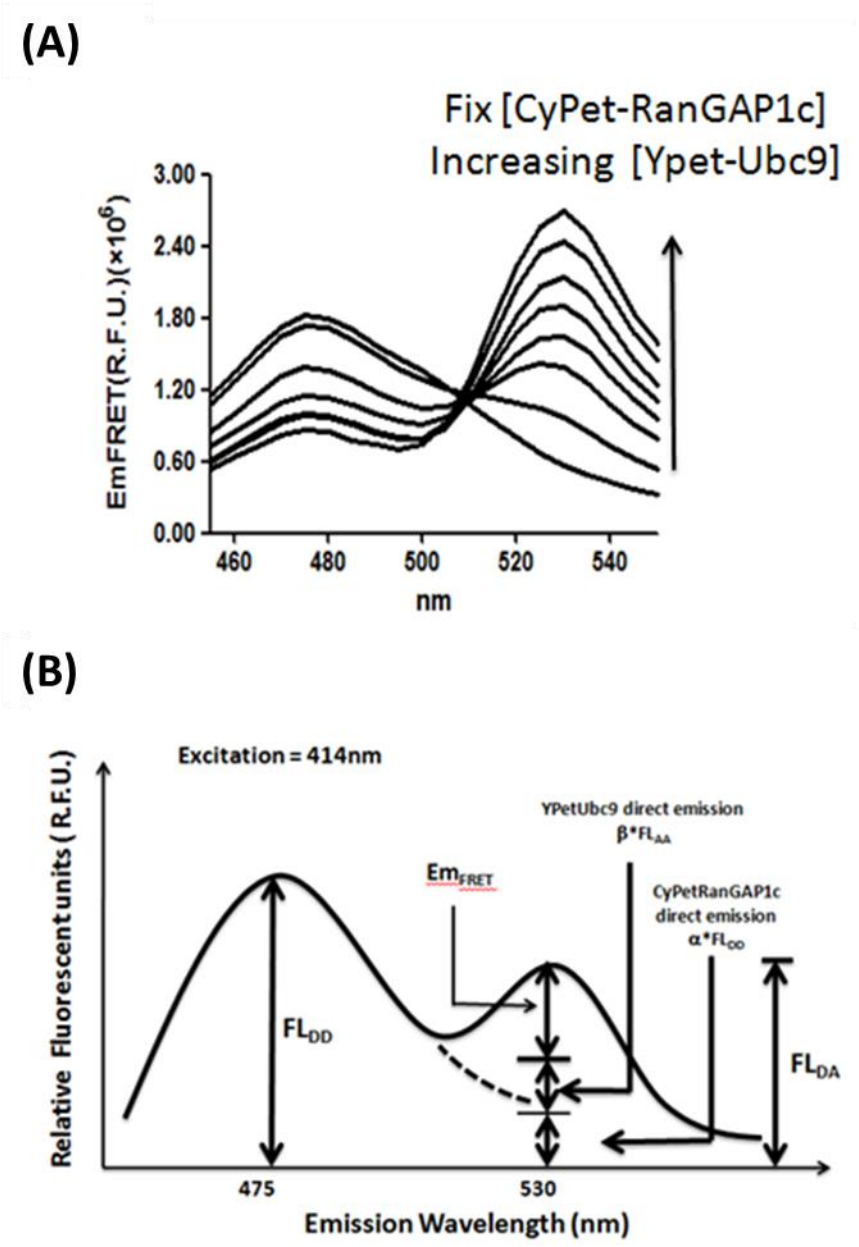

Figure 2.3. Fluorescence signal analysis and titration of FRET signal. (A) The FRET signal titration with increasing concentrations of YPetUbc9. (B) Fractionations of FRET signal.

Table 2.2. K_d results of CyPetRanGap1c with YPetUbc9 under different conditions

CyPetRanGAP1c(μM)	*Kd*(μM)	$Em_{FRETmax}$ (R.F.U.)(x10^4)
0.05	0.098±0.014	1.227±0.022
0.1	0.096±0.013	2.433±0.041
0.5	0.101±0.016	12.29±0.23
1	0.114±0.021	24.61±0.53
0.05+1 μgBSA	0.098±0.022	1.260±0.036
0.1+1μg BSA	0.092±0.024	2.523±0.080
0.5+1 μg BSA	0.105±0.025	12.71±0.38
1.0+1 μg BSA	0.102±0.028	24.97±0.76
0.1+1μg bacterial extracts	0.092±0.022	2.583±0.074
0.1+3μg bacterial extracts	0.092±0.023	2.572±0.079
0.1+10μg bacterial extracts	0.096±0.031	2.636±0.106
0.5+1μg bacterial extracts	0.100±0.027	13.26±0.43
0.5+3μg bacterial extracts	0.108±0.025	13.02±0.39
0.5+10μg bacterial extracts	0.090±0.035	13.07±0.58
1.0+1μg bacterial extracts	0.093±0.031	25.21±0.90
1.0+3μg bacterial extracts	0.109±0.037	25.19±0.99
1.0+10μg bacterial extracts	0.103±0.040	26.06±1.14
0.05 (from crude extract)	0.102±0.024	1.308±0.041
0.1 (from crude extract)	0.100±0.024	2.447±0.075
0.5 (from crude extract)	0.096±0.023	13.57±0.39
1.0 (from crude extract)	0.100±0.029	24.63±0.79
SPR Method *by Ling*	0.097	

(A)

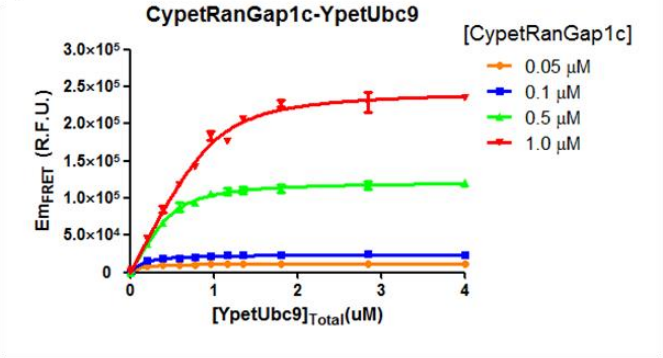
CypetRanGap1c-YpetUbc9
[CypetRanGap1c]
0.05 µM
0.1 µM
0.5 µM
1.0 µM
EmFRET (R.F.U.)
3.0×10⁵
2.5×10⁵
2.0×10⁵
1.5×10⁵
1.0×10⁵
5.0×10⁴
0
0
1
2
3
4
[YpetUbc9]Total(uM)

(B)

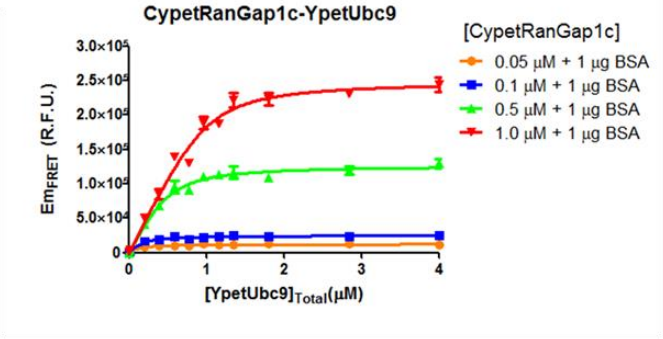
CypetRanGap1c-YpetUbc9
[CypetRanGap1c]
0.05 µM + 1 µg BSA
0.1 µM + 1 µg BSA
0.5 µM + 1 µg BSA
1.0 µM + 1 µg BSA
EmFRET (R.F.U.)
3.0×10⁵
2.5×10⁵
2.0×10⁵
1.5×10⁵
1.0×10⁵
5.0×10⁴
0
0
1
2
3
4
[YpetUbc9]Total(µM)

(C)

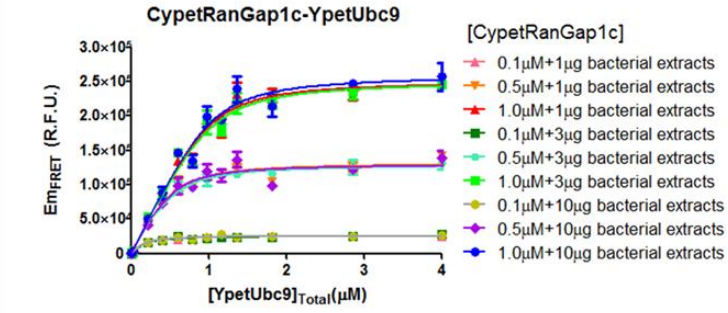
CypetRanGap1c-YpetUbc9
[CypetRanGap1c]
0.1µM+1µg bacterial extracts
0.5µM+1µg bacterial extracts
1.0µM+1µg bacterial extracts
0.1µM+3µg bacterial extracts
0.5µM+3µg bacterial extracts
1.0µM+3µg bacterial extracts
0.1µM+10µg bacterial extracts
0.5µM+10µg bacterial extracts
1.0µM+10µg bacterial extracts
EmFRET (R.F.U.)
3.0×10⁵
2.5×10⁵
2.0×10⁵
1.5×10⁵
1.0×10⁵
5.0×10⁴
0
0
1
2
3
4
[YpetUbc9]Total(µM)

(D)

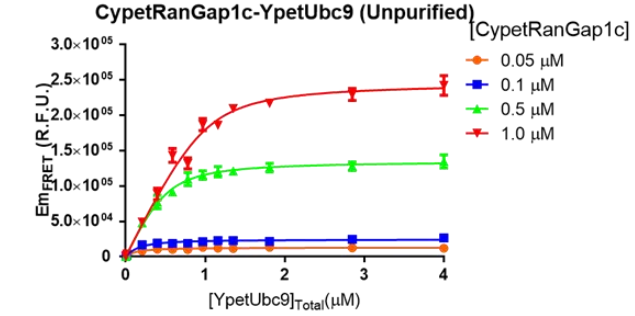
CypetRanGap1c-YpetUbc9 (Unpurified)
[CypetRanGap1c]
0.05 µM
0.1 µM
0.5 µM
1.0 µM
EmFRET (R.F.U.)
3.0×10⁰⁵
2.5×10⁰⁵
2.0×10⁰⁵
1.5×10⁰⁵
1.0×10⁰⁵
5.0×10⁰⁴
0
0
1
2
3
4
[YpetUbc9]Total(µM)

Figure 2.4. Em_{FRET} at different concentrations of purified CyPetRanGAP1c and YPetUbc9 in the presence or absence of other proteins. (A) Graph of Em_{FRET} at 0.05, 0.1, 0.5, 1.0 µM of purified CyPetRanGAP1c with increasing concentration of purified YPetUbc9. (B) Graph of Em_{FRET} at 0.05, 0.1, 0.5, 1.0 µM of purified CyPetRanGAP1c with increasing concentration of purified YPetUbc9 in presence of 1µg BSA. (C) Graph of Em_{FRET} at 0.05, 0.1, 0.5, 1.0 µM of purified CyPetRanGAP1c with increasing concentration of purified YPetUbc9 in presence of 1, 3, 10 µg bacterial protein extracts. (D) Graph of Em_{FRET} at 0.05, 0.1, 0.5, 1.0 µM of unpurified CyPetRanGAP1c with increasing concentration of unpurified YPetUbc9 from crude bacterial extracts.

K_d determination for CyPetRanGAP1c and YPetUbc9 in the presence of BSA or bacterial extract

To verify our assumption that FRET-based K_d determination method can be used for measuring K_d in the presence of contaminate proteins, we determined the K_ds for CyPetRanGAP1c and YPetUbc9, in the presence of BSA or bacterial extract. In each condition, the concentration of CyPetRanGAP1c was fixed to 0.05, 0.1, 0.5 or 1.0 μM, and the concentration of YPetUbc9 was titrated from 0 to 4 μM, in the presence of 1 μg BSA, or 1, 3, 10 μg bacterial extract.

The disassociation constants of CyPetRanGAP1c and YPetUbc9 in the presence of BSA were determined by the non-linear regression as described above. Data sets of Em_{FRET} vs. $[YPetUbc9]_{total}$ were fit in equation (2), and K_ds from different concentrations of CyPetRanGAP1c (0.05, 0.1, 0.5, 1.0 μM) were determined as 0.098±0.022, 0.092±0.024, 0.105±0.025, 0.102±0.028 μM. The average K_d is 0.099 μM, which is consistent with the K_d of 0.102 μM for CyPetRanGAP1c and YPetUbc9 in the absence of BSA.

The disassociation constants of CyPetRanGAP1c and YPetUbc9 in the presence of different amounts of bacterial extract were compared with each other at three concentrations of CyPetRanGAP1c separately. When the concentration of CyPetRanGAP1c was fixed at 0.1 μM, the K_ds were 0.092±0.022, 0.092±0.023 , 0.096±0.031 μM when 1, 3 or 10 μg bacterial extarct was added. When the concentration of CyPetRanGAP1c was fixed at 0.5 μM, the K_ds were 0.100±0.027, 0.108±0.025, 0.090±0.035 μM when 1, 3 or 10 μg bacterial extract was added. When the concentration of CyPetRanGAP1c was fixed at 1.0 μM, the K_ds were

0.093±0.031, 0.109±0.037, 0.103±0.040 μM when 1, 3 or 10 μg bacterial extract was added. The K_ds are very consistent between each group (Table 2.2).

These results suggest that K_ds determined in the absence or presence of BSA or bacterial extract by this method are very consistent and accurate.

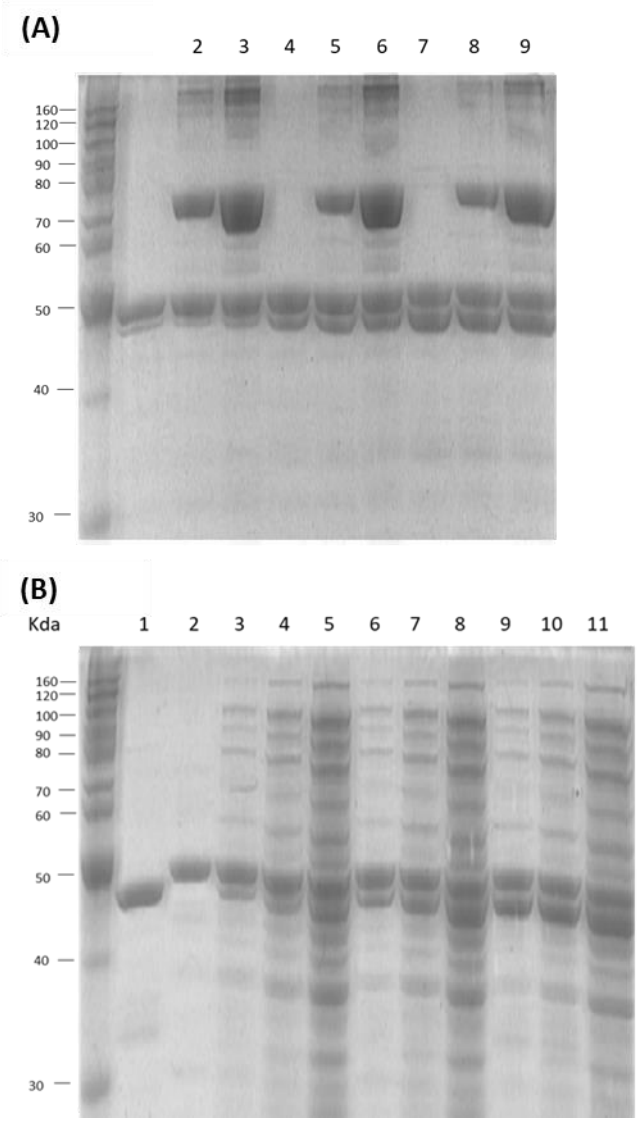
(A)
2 3 4 5 6 7 8 9
160
120
100
90
80
70
60
50
40
30
(B)
Kda
1 2 3 4 5 6 7 8 9 10 11
160
120
100
90
80
70
60
50
40
30

Figure 2.5. SDS-PAGE protein gel of CyPetRanGAP1c and YPetUbc9 under different conditions. (A) The SDS-PAGE protein gel of CyPetRanGAP1c and YPetUbc9 without or with BSA stained with Coomassie. 0.1 μM(lane 1, 2, 3), 0.5 μM (lane 4, 5, 6) or 1.0 μM CyPetRanGAP1c (lane 7, 8, 9) + 1 μM YPetUbc9 without BSA (lane 1, 4, 7), with 1 μg BSA (lane 2, 5, 8), or with 3 μg BSA (lane 3, 6, 9). (B) The SDS-PAGE protein gel of CyPetRanGAP1c and YPetUbc9 without or with *E.coli* cell extract stained with Coomassie. CyPetRanGAP1c (lane 1); YPetUbc9 (Lane 2); 0.1 μM (lane 3,4 and 5), 0.5 μM (lane 6,7 and 8), 1.0 μM (lane 9,10 and 11) of CyPetRanGAP1c + 1 μM YPetUbc9 with 1 μg (lane 3,6 and 9), 3 μg (lane 4,7 and 10), 10 μg (lane 5,8 and 11) of *E.coli* cell extract.

$Em_{FRETmax}$ and K_d determinations in the presence of other proteins

The values of $Em_{FRETmax}$ for CyPetRanGAP1c and YPetUbc9 in the presence of BSA were $(1.260\pm0.036)\times10^4$, $(2.523\pm0.080)\times10^4$, $(12.71\pm0.38)\times10^4$ and $(24.97\pm0.76)\times10^4$, for 0.05, 0.1, 0.5, 1.0 μM of CyPetRanGAP1c, respectively (Table 2.2). The $Em_{FRETmax}$ had a linear relationship with concentration of CyPetRanGAP1c and the curve overlapped with the one without BSA. The values of $Em_{FRETmax}$ for CyPetRanGAP1c and YPetUbc9 in the presence of *E.coli* extract were 2.583±0.074, 13.26±0.43, and 25.21±0.90 when 1 μg bacterial extract was added; 2.572±0.079, 13.02±0.39, and 25.19±0.99 when 3 μg bacterial extract was added; 2.636±0.106, 13.07±0.58, and 26.06±1.14 when 10 μg bacterial extract was added (Table 2.2). The values of K_d and $Em_{FRET\,max}$ are consistent between each group, which indicates our FRET-based method can be used to determine K_d under complicated condition.

To verify the values of K_d from FRET assay, we measured the interaction disassociation constant of CyPetRanGAP1c and YPetUbc9 by SPR. His-tagged YPetUbc9 and CyPetRanGAP1c were expressed in bacterial cells and purified using Ni–NTA agarose beads. After overnight dialysis in BIAcore running buffer, His-tagged YPetUbc9 was immobilized on SPR NTA sensor chip. Non-tagged CyPetRanGAP1c was obtained by thrombin digestion. Non-specific binding of CyPetRanGAP1c to the NTA chip was subtracted based on response signal of control channel of the NTA sensor chip. The binding kinetics analysis showed the binding response of the bound YPetUbc9 to injections of different concentration of CyPetRanGAP1c (Figure 2.7A). CyPetRanGAP1c bound with moderate kinetics to YPetUbc9, with a calculated K_d of 0.097 μM. This K_d was consistent to the K_ds determined by qFRET method as described above. To further analyze the possible interference of

fluorescence tag to the interaction, we performed a control experiment on RanGAP1c and Ubc9 without fluorescent tag. Similar to above experiment, His-tagged Ubc9 was immobilized on NTA sensor chip and RanGAP1c was in flow phase. The binding response of bound Ubc9 to different RanGAP1c concentration showed similar kinetics as the one for fluorescent-tagged proteins (Figure 2.7B). The K_d of RanGAP1c and Ubc9 interaction was calculated as 0.182 μM, which is relatively comparable to the K_d of fluorescent-tagged RanGAP1c and Ubc9.

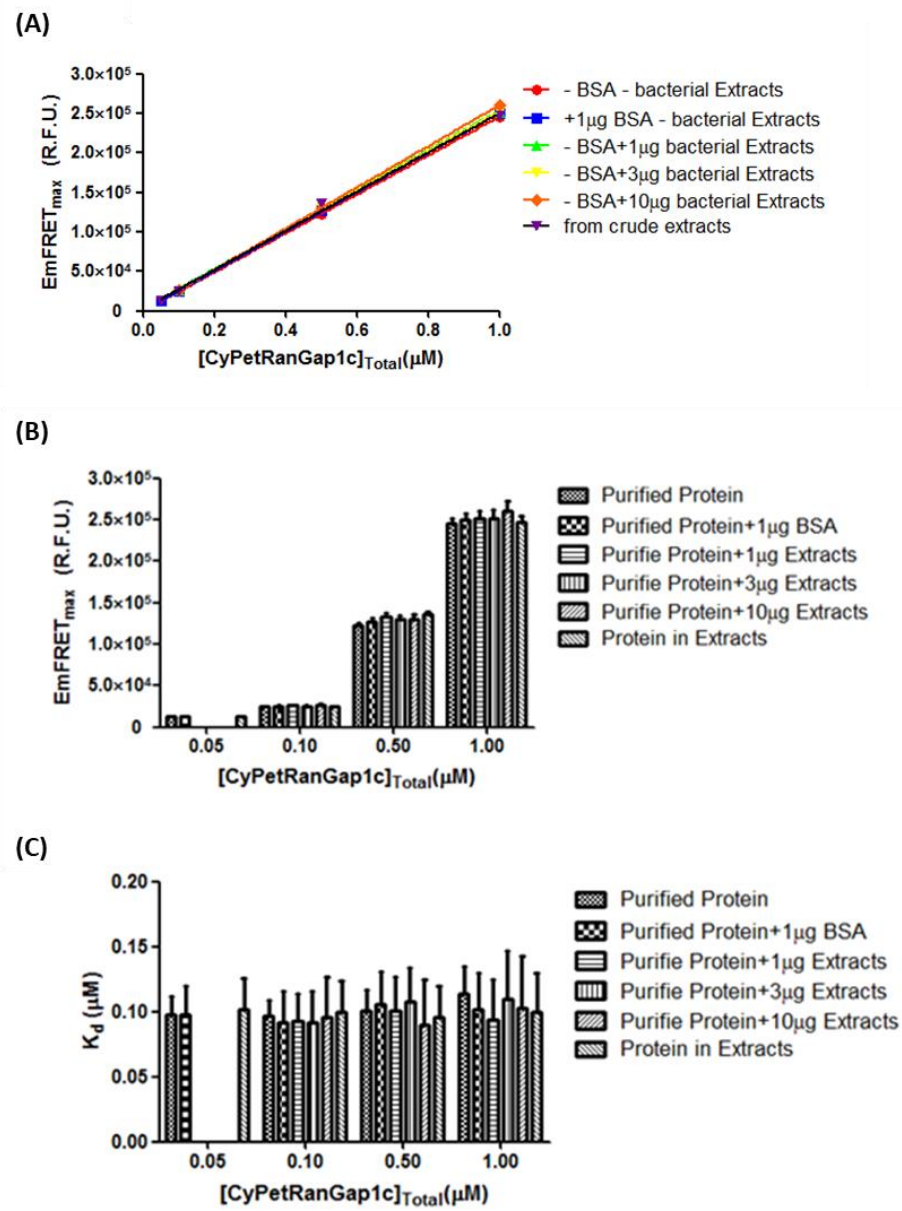

Figure 2.6. $Em_{FRETmax}$ at different concentrations of the donor CyPetRanGAP1c in the absence and presence of other proteins. (A) The maximal FRET emission is proportional to the amount of CyPetRanGAP1c in the assay. (B) Bar graph of $Em_{FRETmax}$ at different concentrations of CyPetRanGAP1c. (C) Bar graph of K_d at different concentrations of CyPetRanGAP1c.

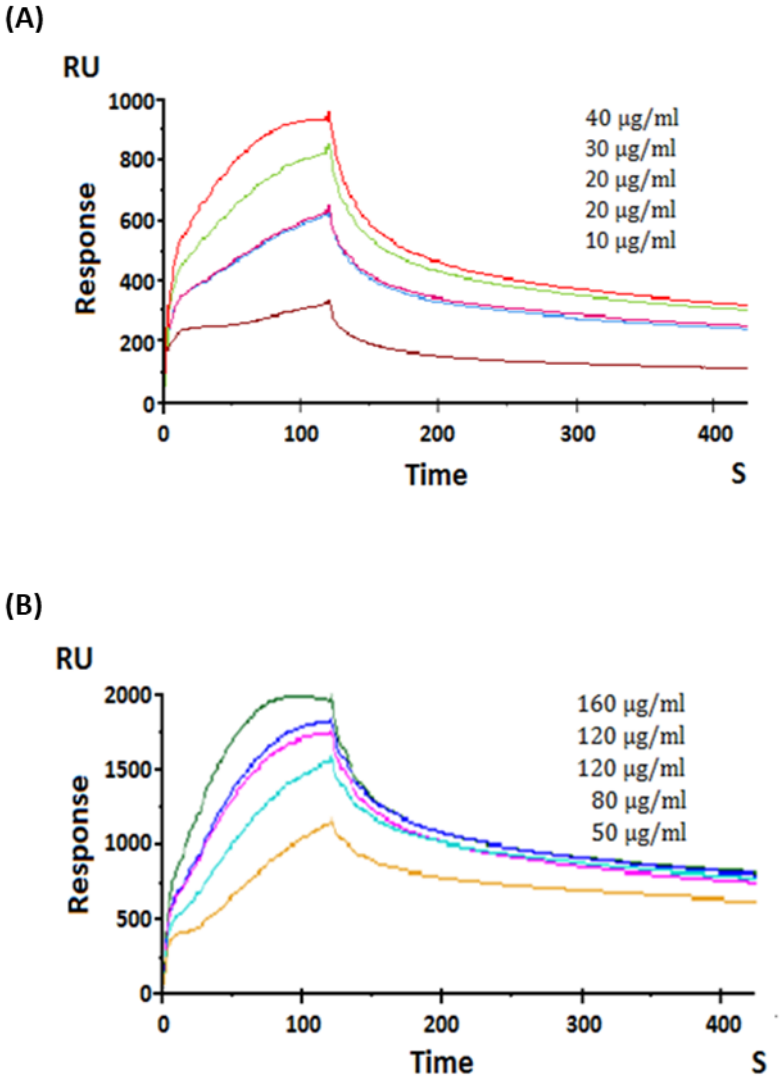

Figure 2.7. Determination of interaction affinity K_d by surface plasma resonance. (A) Determination of K_d between the fusion proteins CyPetRanGAP1c and YPetUbc9 interaction. The K_d is 0.182 µM. (B) Determination of K_d between the Aos1 and Uba2, 0.097 µM.

K_d determination for CyPetRanGAP1c and YPetUbc9 from bacterial crude extract without purification

The concentrations of CyPetRanGAP1c and YPetUbc9 in crude extract were determined using standard curve. The concentration of CyPetRanGAP1c was fixed at 0.05, 0.1, 0.5 or 1.0 μM, the concentration of YPetUbc9 was titrated from 0 to 4 μM. The K_ds were 0.102±0.024 , 0.100±0.024 , 0.096±0.023 and 0.100±0.029 μM for each concentration of CyPetRanGAP1c used in the assay. This result agreed with the one on purified CyPetRanGAP1c and YPetUbc9 (Table 2.2). The values of $Em_{FRETmax}$ were $(1.308\pm0.041)\times10^4$, $(2.447\pm0.075)\times10^4$, $(13.57\pm0.39)\times10^4$ and $(24.63\pm0.79)\times10^4$ which were linearly proportional to the concentrations of CyPetRanGAP1c.

Discussion

Here, we have reported the determination of the disassociation constant, K_d, of the SUMO E2 conjugating enzyme, Ubc9, and the substrate, RanGAP1c by the novel qFRET assay in a single-step experiment. A highly efficient FRET pair, CyPet and YPet, was used to fuse with RanGAP1c and Ubc9, respectively. The K_d results mainly depend on the fluorescence signals which come from the interaction of tagged proteins. This method can be applied to the assay with multiple contaminate proteins in presence and provides quantitative determination of the RanGAP1c and Ubc9 interaction affinity. Without BSA or *E.coli* bacterial extract, the K_d value is 0.102±0.008 μM, determined for various concentrations of CyPet-RanGAP1c ranging from 0.05 to 1.0 μM; In the presence of BSA, the K_d value is 0.102±0.006 μM, determined for various concentrations of CyPet-RanGAP1c ranging from 0.05 to 1.0 μM; In the presence of *E.coli* bacterial extract, the K_d value is 0.098±0.007 μM, determined for various concentrations of CyPet-RanGAP1c ranging from 0.1 to 1 μM; For Crude CyPet-RanGAP1c and YPetUbc9 directly from *E.coli* bacterial extract, the K_d value is 0.099±0.002 μM. These results are very consistent and agree with the K_d value determined by the traditional SPR method (97 nM for CyPet-RanGAP1c and YPet-Ubc9, 182 nM for RanGAP1c and Ubc9). The previous ITC study also showed high affinity interaction between Ubc9 and RanGAP1c (K_d~0.49 μM) (40).

In this research, we verified our results by SPR method, which demonstrates that the novel qFRET assay generates consistent results that agree well with those from other classical K_d measurement methods. Compared with SPR, our FRET-based method has several advantages for determining protein-protein interaction, especially for enzymes.

SPR result is often affected by the potential orientation problem associated with the immobilized protein in assay (41). Also kinetic SPR data can be quite complex due to various effects, including mass transfer effect (42), rebinding effect (43), and nonspecific binding to the sensor chip, and thus careful mathematical analysis is needed to obtain meaningful parameters. This method of K_d determination might not be valid when simple Langmuir-type binding model does not apply (42, 44). In our protein interaction assay, we performed his-tag digestion by thrombin for SPR assay. The thrombin digestion reaction was kept at 16^{o}C to maintain thrombin activity, which might affect the binding affinity of CyPetRanGAP1c and YPetUbc9. Also when we used the BiacoreX100 to get the data, we could only run one sample at one and get relative response in 40 min. So if we run six concentrations in triplicate we need at least 12 hours. However, this can be done in less than one hour by our qFRET-assay.

The dissociation constant, K_d can be determined by many different methods, including fluorometric, surface plasmon resonance (SPR), ITC, radioactive labeling and ultracentrifugation. These methods offer experimental convenience, but also have some disadvantages. They often require expensive instrumentation and multi-step protein purification procedure. Isothermal titration calorimetry (ITC) requires relatively large amount (i.e., micromolar range) of samples and thus might not be suitable for proteins with high interaction affinity (i.e., K_d~5 nM). The elongated centrifugation can perturb the equilibrium between bound and free proteins, especially if the dissociation rates are fast, and thus K_d values determined may not represent true equilibrium constants. Finally, peripheral proteins can be nonspecifically adsorbed on the walls of test tube during high-

speed centrifugation. The intrinsic fluorescence method requires the presence of a tryptophan in the vicinity of proteins binding surface(45-48); tryptophan fluorescence changes might not quantitatively reflect the degree of proteins binding (47); Relatively low sensitivity of the method entails the use of micromolar protein concentrations for assay. The FRET method in general is more sensitive than the intrinsic fluorescence measurement and offers more flexibility in assay design. Although the FRET method shares the same drawbacks with the intrinsic fluorescence measurement, using fluorescence protein can deal with these problems.

The high-affinity interaction of RanGAP1c and Ubc9 may provide explanations of how Ubc9 mediates SUMO conjugation to RanGAP1c directly without E3. The crystal structure of RanGAP1c-Ubc9 shows critical interactions between two molecules that provide the molecular basis for recognition of the RanGAP1c Ψ-K-X-D/E consensus motif. The interface can be divided in two parts. One is between RanGAP1c helices H and F and Ubc9 surface emanating mainly from helix C. The second part includes interactions between the consensus RanGAP1c SUMOylation motif (-LKSE-) and Ubc9 surface that includes the catalytic cysteine, strands 6 and 7, and the loop preceding helix C (49). These interactions likely lead to an increased binding and more effective SUMO transfer. Our experiment demonstrated the high-affinity interaction of RanGAP1c-Ubc9 by the qFRET based assay.

The consistent results of the K_d determination at nanomolar range not only show that our method is accurate and reliable at various concentrations of the interactive partners but also sensitive at high affinity nanomolar level. In contrast, traditional radioisotope-labeled protein binding assay to determine K_d requires a range of at least 100-fold of labeled

ligand to predict maximum binding. Our FRET-based K_d determination approach accurately determines K_d at ratios 0.67–40 fold of the binding partners of the RanGAP1c-Ubc9. Other approaches for K_d determination, such as SPR or isothermal titration calorimetry, require multiple steps and special instruments and often give large variations. While the FRET assay has become more popular in biochemical and cell biology studies, our qFRET method would advance FRET technology to another quantitative level, and information on RanGAP1c-Ubc9 interaction affinity will provide valuable insights into the complex UBL conjugation cascade from systems biology perspective.

CHAPTER 3: Development of Quantitative FRET Technology for K_i Determination and its Application for Characterization of a Small Molecule Inhibitor of SUMOylation

Abstract

The potency of enzyme inhibitor is characterized as the inhibition constant, K_i. Small Ubiquitin-like Modifier (SUMO) modification is a post-translational modification affecting many cellular processes, including nuclear transport, transcriptional regulation, cell cycle progression, and protein stability. SUMO modification regulates activities of a wide array of proteins, for example the repression of p53 in the tumor suppression pathways and STAT1 in interferon γ-mediated antivirus activity. SUMOylation inhibitors can serve as potential anticancer and antivirus reagents. Recently, we have identified a small molecule inhibitor of SUMOylation at its E1 activating enzyme via FRET-based high-throughput screening. Here we report a systematic development of quantitative FRET-based methodology for K_i determination and inhibition type characterizations. Our results show that STE is a non-competitive inhibitor with K_i ~0.67 μM. The characterization of STE and its derivatives may lead to improved therapeutic modalities for cancers and several infectious diseases. The novel development of FRET-based enzyme kinetics and inhibitor characterizations can be expanded to other enzymes in general and represent a novel technology development of enzyme kinetics.

Introduction

SUMOylation is an important post-translational modification in eukaryotes that is involved in a variety of physiological processes. The SUMO modification of target protein can alter its transcriptional activity, cellular translocation, protein-protein interaction, and stability. SUMOylation is a multi-step enzymatic cascade that involves the sequential reactions of E1 (Aos1/Uba2), E2 (Ubc9) and E3 ligases (3). The SUMO cycle starts from precursor SUMO being processed by SENPs and activated by SUMO E1 with a thioester bond formation between catalytic cysteine of E1 and C-terminus of SUMO. Then the SUMO E2 will catalyze a trans-thiolation reaction, resulting in a thioester bond formation between catalytic cysteine of E2 and SUMO1. After that, SUMO will be eventually transferred to the lysine residues of substrate proteins with the help SUMO E3s. SUMO can also be cleaved from the substrates with the action of SENPs. It is proven in many cases that SUMOylation has significant roles in carcinogenesis, viral replication and neurodegenerative diseases (50, 51). These results support that SUMOylation can be a novel target for developing new therapeutic strategies. Despite its critical role in many pathological processes, detailed mechanism of how SUMO pathway regulates different physiological processes is yet understood.

Traditional genetic approaches of studying the biological function of SUMO pathway by gene knockout have been shown to be quite difficult, since the modification of SUMO is essential for a wide range of physiological processes, including regulating immune signal pathway, chromosome segregation, and maintaining nuclear architecture and function. Depletion of SUMO1 or Ubc9 can cause severe cellular defects resulting in

embryonic lethality (16, 17). Mice that are deficient of SUMO E3 PIAS1 have much lower production rate (18). To overcome this challenge, new strategy needs to be implemented to study the mechanism of SUMO pathway. Compared to traditional biochemical and genetic approaches, the utilization of small chemical compounds provides great advantages for studying biological processes. A bioactive small compound which in many cases is a specific enzyme inhibitor can be easily implemented to study the biological process in time-course or dose-response manner. It is also valuable for understanding enzymatic mechanism and development of new therapeutic strategy.

Up to date, less than ten small chemical compounds that inhibit SUMO pathway have been reported (Table 3.1). Two most widely used SUMOylation inhibitors, ginkgolic acid and kerriamycin B are also the first two reported inhibitors identified from natural products (52, 53). However, they were showed to inhibit the activities of a wide range of enzymes, and cause severe side effects, including inhibition of histone acetylation and G+-bacterium (54). It is also found that ginkgolic acid which is the most commercially available SUMOylation inhibitor and only one under clinical study, exhibits varied efficacy from different assay and substrate being tested (55-57). Recently, our group has discovered a novel small chemical SUMOylation inhibitor-STE through a FRET-based high-throughput screening assay. Further characterization of this compound may lead to new therapeutic agent for cancer and virus infection treatment.

FRET occurs between two adjacent fluorophores when their distance over distances from ~1–10nm and the non-radioactive energy transfer from excited donor to acceptor through dipole-dipole coupling. Since the energy transfer efficiency is strongly dependent

(sixth-power) on the distance between the FRET donor and accepter, FRET-based technique has great advantage on studying intermolecular interaction. Our group has systematically established qFRET-based strategy for the determination of biochemical parameters, such as protein interaction affinity (38), and enzymatic kinetics (58-60). These new developments have several advantages over traditional biochemical approaches for determining biochemical parameters. These approaches are proven to be very precise and provide comparable results to those from traditional methods in a more cost-effective and time-saving manner. Besides, the FRET signal can be tracked continuously along the reaction progress, and this technique is straightforward and environment-friendly. In this study, we further developed qFRET assay for charactering inhibitor type and determination of inhibition constant.

Table 3.1. List of SUMOylation inhibitors by different groups

Compound	Target	IC50 (μM)	Reference
Ginkgolic acid	E1	3.0	(Fukuda et al., 2009a)
Kerriamycin B	E1	11.7	(Fukuda et al., 2009b)
2-D08	UBC9	6.0	(Kim et al., 2013)
GSK145A	UBC9	12.5	(Brandt et al., 2013)
Spectomycin	UBC9	4.4	(Hirohama et al., 2013)
C#21	E1	14.4	(Kumar et al., 2013)
Davidiin	E1	0.15	(Takemoto et al., 2014)
Tannic acid	E1	12.8	(Suzawa et al., 2015)
ML-792	E1	0.003	(He et al., 2017)

An appropriate enzyme assay is important to identify a special enzyme and to understand its enzymatic kinetics. The method for observing an enzyme reaction highly depends on the observed feature of substrate and product for specific enzyme. A relatively easy approach with low susceptibility against disturbance is photometric assay (61, 62). Although it is the most widely used method, it requires substrate and product have distinct absorbance spectra, and often generates results with low accuracy due to poor sensitivity of absorbance measurement. Compared to that, fluorimetry-based method is about hundredfold more sensitive, but very limited enzymatic substrates or products have detectable fluorescence spectra, e.g. NADH (61, 63). Besides optical methods, electrochemical methods are commonly used, e.g. pH measurement for reactions with pH changes. However, pH changes can influence enzyme activity severely, thus the reaction proceeding is often measured by tracking the amount of neutralizing reagent added to keep the pH constant, which causes more sources of errors (64). Overall, all the methods mentioned above allow continuous track of the reaction proceeding in which a complete progress curve can be observed, but they require direct signal from substrate or product which can be measure in real-time. And when this requirement cannot be fulfilled, a coupled indicator reaction or a separation method need to be performed to analyze the amount of product generated or substrate consumed at a defined time. These often require a termination of the reaction at a specific time point, and thus can only provide one single point for calculating the reaction velocity. But there is no guarantee that the measurement occurs within the linear part of the reaction proceeding curve. To overcome these problems, we have developed qFRET-based enzymatic assay which is based on the real-time

measurement of FRET signal correlated with the amount of substrate binding or cleavage. This method offers several advantages including high sensitivity, less labor and time needed and applicability to various types of enzymatic reactions.

A comprehensive study of enzyme inhibition helps elucidate the fundamental knowledge of enzyme structure, including the physical and chemical micro-environment around the active site, the enzyme-substrate and enzyme-product intermediates. It also provides valuable information on the cellular regulation of the metabolic pathway and pharmacological practices. Many existing drugs and research probes are reversible inhibitors, which are usually classified into three modes: competitive, noncompetitive and uncompetitive (65). The inhibition constant K_i and K_i' are commonly used to characterize the corresponding inhibition process. The traditional way for analysis of the kinetic data consists of several steps, including data acquisition, plot inspection, kinetic model construction, derivation of kinetic equation, and regression analysis (66). The most frequently used data analysis method is Dixon plot, which converts a nonlinear relationship to linearized form, and thus provides unreliable estimates of K_i in many cases (67, 68). In comparison, simultaneous nonlinear regression (SNLR) which directly fits all data simultaneously to the nonlinear inhibition model is proven to be a more reliable method. Here, we have developed a robust strategy for K_i determination which combines our qFRET assay with improved SNLR method, and utilized this method to characterize our newly discovered SUMOylation inhibitor-STE.

Materials and Methods

Molecular cloning of DNA constructs

The recombinant expression constructs of pET28(b)-CyPet-SUMO1, pET28(b)-YPet-Ubc9, pET28(b)-Aos1, pET28(b)-Uba2 were cloned as described before (38, 69). For creating pET28(b)-CyPet-SUMO1 and pET28(b)-YPet-Ubc9, the FRET pair genes (CyPet/YPet) were amplified by PCR and flanked with NheI and SalI sites on both ends. The open reading frames of SUMO1 and Ubc9 were amplified by PCR with SalI and NotI sites on both ends. Then CyPet/YPet fragment and SUMO1/Ubc9 fragment were digested by NheI/SalI and SalI/NotI respectively, and inserted into the multi-cloning site of bacterial expression vector-pET28(b). The recombinant constructs were confirmed by DNA sequence alignment.

Production and purification of His-tagged proteins

pET28(b) plasmids encoding CyPet-SUMO1, YPet-Ubc9, Aos1, Uba2 created above were transformed into BL21 (DE3) *E. coli*. The transformed bacterial stocks were inoculated in LB medium and then expanded in 2XYT medium. The production of polyhistidine-tagged proteins was induced by adding 0.3 mM IPTG and the medium was shaken at 25 °C overnight. The recombinant proteins were purified with Ni_2^+ -NTA agarose beads (QIAGEN) and then dialyzed in buffer containing 20 mM Tris-HCl (pH=7.4), 50 mM NaCl and 1 mM DTT. The proteins generated above were loaded on the SDS-PAGE with Coomassie blue staining afterwards for checking purity and their concentrations were measured by Bradford assay with known amounts of bovine serum albumin as standards.

In vitro FRET assay for STE inhibition of SUMO E1

A dose-response *in vitro* FRET assay was first set up to verify the SUMOylation inhibition effect of STE. To achieve that, 0.75 μM CyPet-SUMO1, 2 μM YPet-Ubc9, 20 nM Aos1, 20 nM Uba2 were mixed in SUMOylation buffer (50 mM Tris-HCl, pH 7.4, 4 mM $MgCl_2$, 1 mM DTT), with addition of DMSO as control or serial concentrations of STE (0.16, 0.31, 0.63, 1.25, 2.50, 5.00, 10.00, 20.00 μM) in a total volume of 60 μL. The sample mixtures were incubated in a Greiner 384-well plate (Sigma-Aldrich) at 37 °C for 10 min. Then 1 mM ATP was added to each reaction, and fluorescence emissions were measured in time course using FlexstationII384 (Molecular Devices). The fluorescence emissions under three wavelength settings (Excitation/ Emission, Ex/Em) were recorded: Ex 414 nm/ Em 475 nm, Ex 475nm/ Em 530 nm, Ex 414 nm/Em 530nm, which represent direct emission from CyPet, YPet and total FRET signal respectively. To further obtain the kinetic parameters $V_{max,}$ $K_{m,}$ K_i of SUMO E1, twelve substrate concentrations (0, 0.2, 0.3, 0.4, 0.5, 0.7, 0.9, 1.3, 1.7, 2.3, 3.0, 4.0 μM) were paired separately with DMSO as control or three inhibitor concentrations (0.2, 0.8, 2.0 μM). All metabolic formation rates were tracked in triplicate, and corresponding fluorescence signals were averaged for each condition.

Data analysis and K_i determination

The emission intensities from each reaction were first calibrated by subtracting the background signals from the blank plate. Then the absolute FRET signal (Em_{FRET}) was calculated by subtraction of direct contributions from donor-CyPet and acceptor-YPet, as described previously (38). Next, the data set of Em_{FRET} versus reaction time for each

substrate and inhibitor concentration pair was fitted in one phase association curve to determine the corresponding initial velocity (V_0) using GraphPad Prism (GraphPad Software). After generating the data set of V_0 under each substrate and inhibitor concentration pair, the kinetic parameters V_{max}, K_m, K_i of SUMO E1 were estimated by direct non-linear regression.

Results

Development of qFRET assay to measure SUMO E1 enzyme kinetics and K_i

E1-catalyzed conjugation of SUMO with Ubc9 involves three reactants: ATP, SUMO and Ubc9 (Figure 3.1A). This reaction is considered a pseudo-first order reaction with respect to SUMO as the only substrate when ATP and Ubc9 are held at constant, excess concentration (65). To design the SUMO E1 kinetic experiments, various concentrations of CyPet-SUMO1 were mixed with constant concentrations of other reaction components. A FRET pair CyPet and YPet which exhibits twenty-fold higher FRET efficiency than the original CFP-YFP pair (23) were fused to SUMO1 and Ubc9 respectively through the molecular cloning strategy. The SUMO E1-catalyzed formation of the thioester bond between C-terminal glycine residue of SUMO1 and active cystine residue of Ubc9 will bring the fused FRET pair to a close proximity which allows efficient Förster Resonance Energy Transfer. This can be detected as a significant increase of emission intensity over time at 530 nm when the sample is excited at 414 nm (Figure 3.1B). The total FRET signal (Em_{total}, Ex 414nm/ Em 530 nm) can be differentiated into three fractions: absolute FRET emission (Em_{FRET}), CyPet direct emission and YPet direct emission. Our group has previously developed a spectrum analysis method to determine absolute FRET emission (EmFRET) through three-wavelength measurement. In this method, the CyPet and YPet direct emissions are calculated by multiplying the fluorescence signals of CyPet (FL_{DD}, Ex 414 nm/ Em 475 nm) and YPet (FL_{AA}, Ex 475 nm/ Em 530 nm) by their corresponding ratio factors (x = 0.378, y = 0.026). Em_{FRET} is

obtained by subtracting the fluorescence contributions of CyPet and YPet as described above from Em_{total}.

$$Em_{FRET} = Em_{total} - x * FL_{DD} - y * FL_{AA} \quad (1)$$

Data analysis of real-time Em_{FRET} which is correlate with the amount of conjugated CyPet-SUMO1 and YPet-Ubc9 is performed to further calculate the enzyme kinetics parameters.

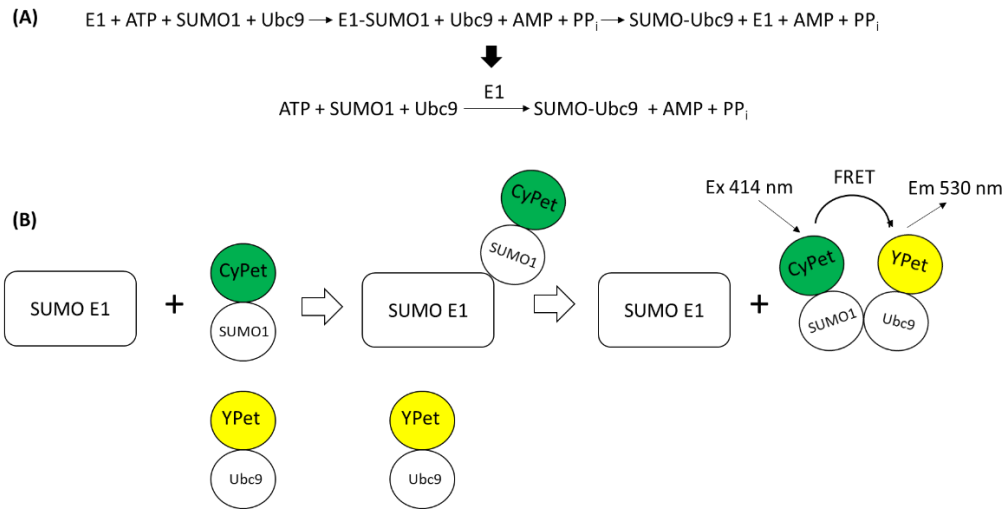

Figure 3.1. A qFRET assay to measure kinetics of the E1 enzyme in the SUMOylation pathway. (A) Reaction scheme of the initial velocity measurement. (B) The kinetic measurement is based on changes in the FRET signal by measuring the fluorescence emission intensity at 530 nm.

Determining the initial velocity of SUMO E1 with SUMO1 as substrate

The steady state E1-catalyzed CyPet-SUMO1~YPet-Ubc9 conjugation can be monitored by tracking the changes of absolute FRET emission (Em_{FRET}) during the reaction. Here, we utilize the pseudo-first order kinetics to calculate the E1 enzyme kinetics for CyPet-SUMO1 under saturated concentration of YPet-Ubc9 and ATP. The product concentration will increase exponentially from t=0:

$$p = [CyPet-SUMO1]_{Total}(1-e^{-kt}) = x(1-e^{-kt}) \quad (2)$$

With the assumption that product concentration is linearly correlated to Em_{FRET}, the data set of Em_{FRET} versus time can be fitted in one-phase association to obtain the best-estimate value of rate constant k.

Accordingly, the initial velocity (V_0) represents the rate the product formation at t=0:

$$V_0 = \frac{dp}{dt_{t=0}} = kx \quad (3)$$

Data analysis and V_{max}, K_m, K_i determination

There are three major forms of reversible inhibitor interactions with enzymes: competitive, noncompetitive and uncompetitive inhibition, which refer to the cases in which an inhibitor exhibits binding affinity exclusively to the free enzyme, to both the free enzyme and enzyme-substrate complex, and exclusively to the enzyme-substrate complex, respectively (Figure 3.2A). The binding capacity of an inhibitor to the free enzyme and enzyme-substrate complex are quantified by measuring the two respective inhibition constants K_i and $K_i'(\alpha K_i)$ (Figure 3.2B). A customized Michaelis-Menton equation was

used for simultaneous nonlinear regression (SNLR), in which the initial velocity at different substrate and inhibitor concentrations were fitted in the model for determining the best-fit values of $V_{max,}$ $K_{m,}$ K_i (Figure 3.2C)(65).

(A)

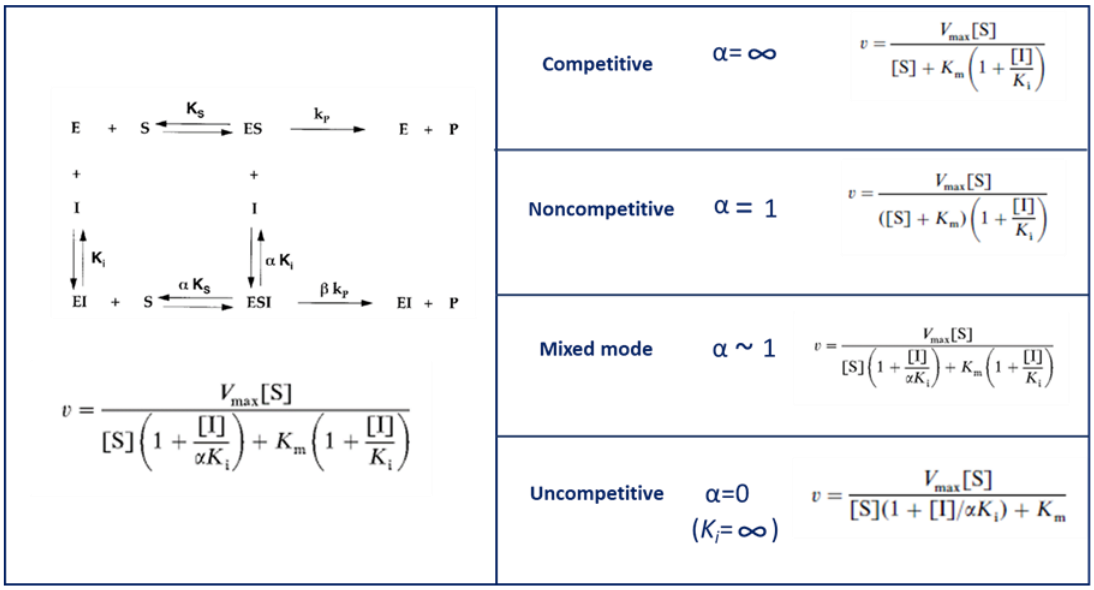

(B)

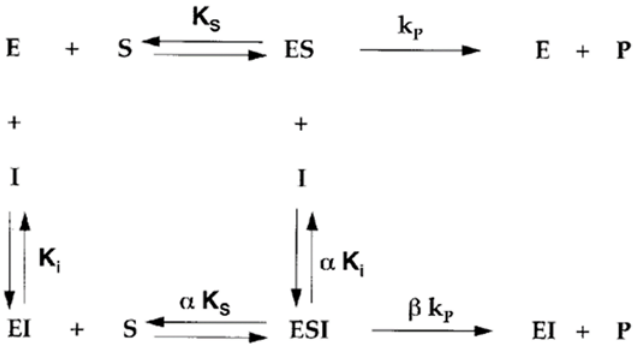

(C)

$$v = \frac{V_{max}[S]}{[S]\left(1+\frac{[I]}{\alpha K_i}\right)+K_m\left(1+\frac{[I]}{K_i}\right)}$$

Figure 3.2. Equilibrium treatment of reversible inhibition. (A) Four modes of reversible enzyme inhibition. (B) equilibrium scheme of enzyme turnover in the presence and absence of an inhibitor. (B) The general velocity equation for an enzymatic reaction in the presence of an inhibitor

STE inhibits SUMO E1 activity in a dose-dependent manner

Our group has previously developed FRET-based high throughput screening platform to identify new SUMOylation inhibitors, and has successfully found STE as the most potent compound with IC_{50} value of 1.6 μM. Here, we established the *in vitro* SUMO E1 enzymatic assay and tested the effect of STE under various concentrations with fixed concentrations of SUMO E1 and substrates. Em_{FRET} was calculated at each time point and the data set was plotted with one-phase association fit to determine the initial velocity under treatment of different STE concentration (Figure 3.3B,C). The reaction mixes were also run on western blot with anti-SUMO1, and band intensities of CyPet-SUMO1~YPet-Ubc9 conjugates were displayed to represent relative amounts of product formation after 0.5h reaction (Figure 3.3A). The initial velocity of SUMO E1 enzymatic reaction in the presence of different concentration of STE shows a dose dependent manner. Compared to traditional western blot-based SUMOylation assay, our FRET strategy generates more accurate data and requires less time and efforts.

(A)

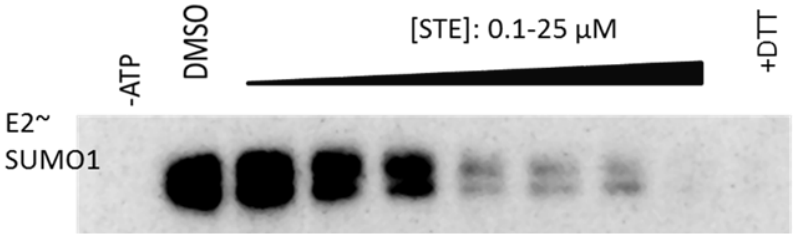
-ATP
DMSO
[STE]: 0.1-25 μM
+DTT
E2~
SUMO1

(B)

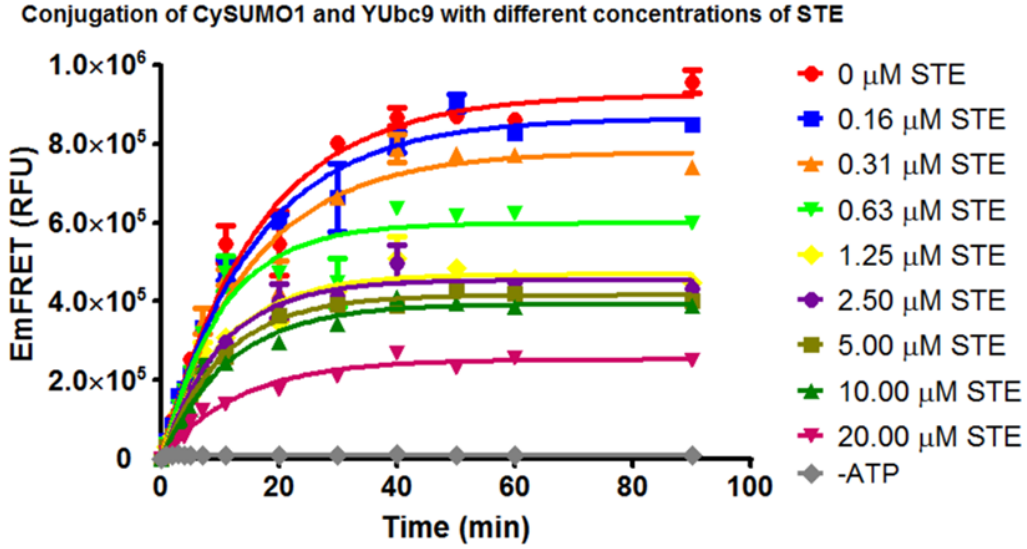
Conjugation of CySUMO1 and YUbc9 with different concentrations of STE
EmFRET (RFU)
1.0×10^6
8.0×10^5
6.0×10^5
4.0×10^5
2.0×10^5
0
0
20
40
60
80
100
Time (min)
0 μM STE
0.16 μM STE
0.31 μM STE
0.63 μM STE
1.25 μM STE
2.50 μM STE
5.00 μM STE
10.00 μM STE
20.00 μM STE
-ATP

(C)

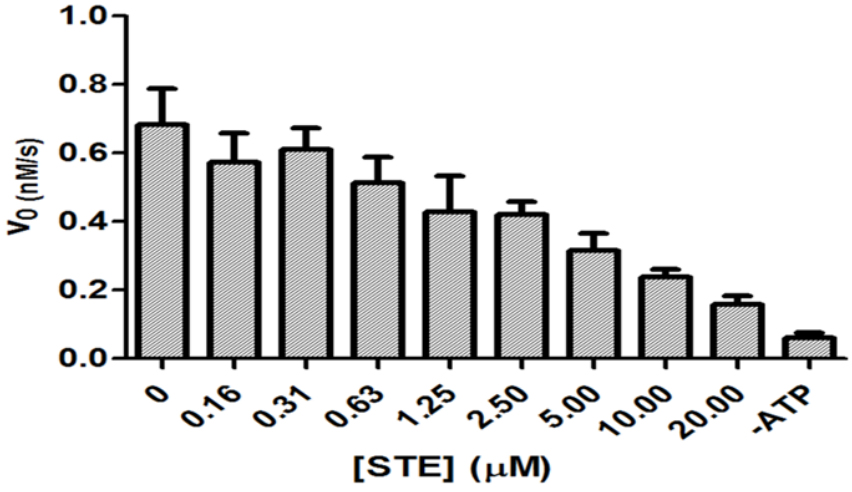
V0 (nM/s)
1.0
0.8
0.6
0.4
0.2
0.0
0
0.16
0.31
0.63
1.25
2.50
5.00
10.00
20.00
-ATP
[STE] (μM)

Figure 3.3. STE inhibits SUMO E2 thioester formation in a dose dependent manner *in vitro*. The *in vitro* SUMOylation assay is initiated by adding 0.1 μM ATP to the reaction mix (0.75 μM CypetSUMO1, 2 μM YPetUbc9, 20nM SUMO E1 in SUMOylation buffer). The amount of CypetSUMO1-YpetUbc9 conjugate produced in presence of different concentrations of STE was estimated by (A) western blotting using anti-SUMO1 and (B) measuring the absolute FRET increase over time. (C) initial velocity was converted by the Em_{FRET} increase in the first 2min divided by the Em_{FRET}-conjugate concentration ratio.

Characterization of inhibition type and inhibition constant of STE by qFRET assay

STE has been previously found to inhibit SUMO pathway both *in vitro* and *in vivo*, and further result suggests STE targets E1-SUMO1 thioester formation with IC_{50} at 1.60 μM. We followed conventional experimental design for evaluation of mechanism of SUMO E1 inhibition with STE. Twelve Cypet-SUMO1 concentrations which were reported previously (60) were paired separately with DMSO as control or three inhibitor concentrations (low, medium and high). All reaction mixes were tracked in triplicate, and fluorescence signals were averaged before data processing. The averaged Em_{FRET} versus time was fitted in one-phase association to obtain individual initial velocity value (V_0) for each of the substrate and inhibitor concentration combinations. Thus, totally 48 data points of V_0 for each substrate-inhibitor concentration pair were generated and fitted in mix-mode inhibitor equation with global fit setting by GraphPad Prism 5 to estimate the best fit values for $V_{max,}$ $K_{m,}$ K_i and K_i' (Figure 3.4A). The result shows STE binds to free E1 and E1-SUMO1 intermediate complex at relatively same level (K_i = 0.67 μM, K_i' = 0.58 μM), which suggest STE is noncompetitive inhibitor for SUMO E1.

(A)

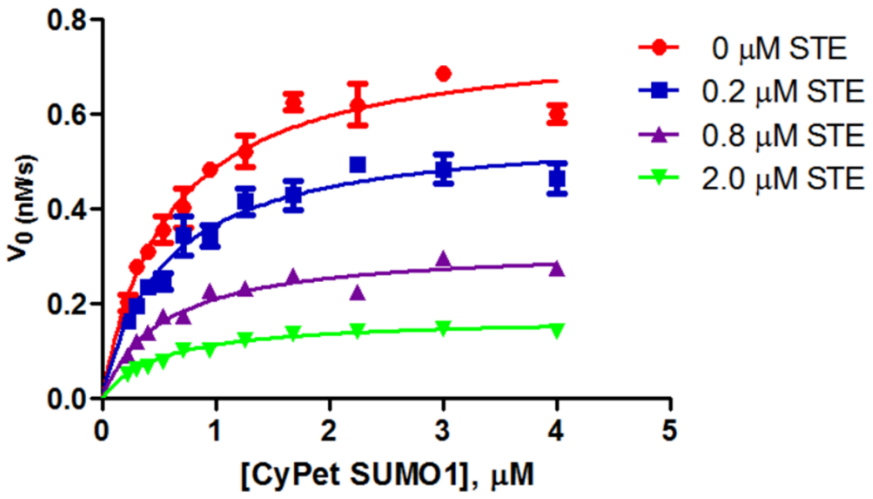

(B)

K_i (µM)	α	K_m (µM)	k_{cat} (s^{-1})
0.67±0.14	0.86±0.24	0.58±0.04	38±1

Figure 3.4. Enzyme kinetics of SUMO E1 in the absence and presence of different concentrations of STE. (A) Determining the initial velocity of in vitro SUMOylation reaction by correlating the absolute FRET with CypetSUMO1-YpetUbc9 conjugate concentration. (B) The best-fit values of $V_{max,}$ $K_{m,}$ K_i and α were estimated by global fit nonlinear regression using equation.

Discussion

In this study, we have systematically developed qFRET technology for determining the mechanism of E1 enzyme inhibition, and used this strategy to characterize the type of STE inhibition and its inhibition constant. QFRET assays have been taken forward for a series of biochemical parameter determinations in real time. This new development has several advantages over other traditional biochemical and biophysical approaches for these biochemical parameter determinations, e.g. the qFRET-based technology is environmentally friendly, provides real-time signal and can be easily converted to high-throughput assay format. In the current mathematical model, the real-time absolute FRET signal is first converted to initial velocity, and the initial velocity is further fitted in a Michaelis-Menten model for estimating K_i and α values. Our most recent study has developed a robust model which correlates the K_i and α values with raw FRET signal in one step. We propose to convert this qFRET-based methodology into an automatic platform which can be easily adapted in academic and industry. We believe this method can be adapted to fulfill the demand of high-throughput platform that can be used to routinely screen a very large number of new chemical entities with a wide range of enzymes and substrates.

To understand the inhibitor-protein interaction and to develop novel therapeutic agent, it is important to understand mechanism of enzyme inhibition. To determine the inhibition type and inhibition constant, data from biochemical assay is most commonly analyzed through linearized form of nonlinear relationship. The most frequently used methods were developed by Lineweaver-Burk (70) and Dixon (71), that rely on linearized

versions of the Michaelis-Mention kinetics model. The Lineweaver-Burk double-reciprocal method can generate very inaccurate result because the high substrate concentration data points are crowded in the area that is close to ordinate axis in the linearized form. The replot of slope and intercept will further magnify the variations in determining inhibition constant. The graphic method of Dixon also can produce substantial errors and is not applicable to partial inhibition mode. Nimmo and Atkins were the first to report the advantages of using simultaneous nonlinear regression (SNLR), in which all data is directly fit to the nonlinear inhibition equation (72). In this report, we have taken the advantage of SNLR and incorporate it in our FRET data analysis and develop a robust and reliable strategy for determining enzyme inhibition kinetics.

We have characterized STE as a non-competitive inhibitor on SUMO E1 with K_i ~0.67 μM, α~0.86. This suggests that STE binds to an allosteric site of E1 enzyme and may interfere with the conformational changes of E1 necessary for activation of SUMO. In addition, STE may serve as a lead structure for the design of more potent analogues. Affinity and selectivity can be improved by ensuring more perfect geometric and noncovalent interactions with the binding site.

CHAPTER 4: Discovery and Characterization of SUMOylation Site of NS1 Protein in Influenza Viral Life Cycle Using FRET Technology

Abstract

The influenza A virus is responsible for the deaths of over 600,000 people each year. The nonstructural protein 1 (NS1) of the influenza A virus is one the major factors which contribute to the virulence of the seasonal influenza A virus. NS1 has been shown to interact directly with the host SUMOylation cascade and interfering the host viral defense mechanisms. In this study, we demonstrate that the lysine residue K131 in the effector domain of NS1 is identified as SUMO acceptor site through a novel FRET-based approach. Furthermore, the growth rate of H1N1 influenza A (A/PR/8/34) with the SUMOylation-deficient NS1 mutant was significantly reduced compared the wild-type virus. Together, these results indicate that NS1 SUMOylation promotes rapid replication of influenza virus, and the interaction of NS1 with SUMOylation components may serve as novel antiviral drug target, due to the well-known function of NS1 for inhibition of host immune responses.

Introduction

Seasonal epidemics or pandemics of the flu have been a global burden since the beginning of modern medicine. These localized epidemics and global pandemics are caused most commonly by the influenza A virus. The influenza A virus utilizes aquatic fowl as its primary reservoirs which can later be used to cross species barriers to infect livestock and humans and cause a highly infectious disease with severe morbidity and mortality (73, 74). In addition, new strains of the influenza virus are assembled through these opportunistic events with antigenic mutation or reassortment, potentially leading to the outbreak of new, more lethal strains that can also harbor drug-resistant genes, which may result in unexpected world-wide pandemics such as the "swine flu" 2009 H1N1 and "bird flu" 2013 H7N9. Besides that, the annual epidemics cause about 3 to 5 million cases of severe, and about 290 000 to 650 000 deaths per year based on the most recent WHO study (75, 76).

The influenza A virus is a negative sense single-stranded RNA virus composed of eight segments that encode more than 12 proteins. Each protein plays a special part in the viral lifecycle, orchestrating the viral entry, protein expression, and viral replication. The virus begins as an enveloped RNA virus with the hemagglutinin (HA) surface glycoproteins binding to sialic acid on the surface of a host cell. The preference of the virus towards the 2,3-linkage of sialic acid on galactose or 2,6-linked sialic acid is an indicator of the origin of the virus. Viruses that originated from avian or equine species prefer the 2,3-linked sialic acid whereas viruses that originate in humans prefer the 2,6-linked sialic acids but swine viruses bind both linkages of sialic acid (77). After the virus binds to the

cell surface, it is endocytosed into a vesicle. During the early endosomal formation, the viral M2 proton channels allow for the acidification of the viral interior, inducing conformational changes of the HA proteins, resulting in the fusion of the viral membrane and the endosomal membrane (78). After membrane fusion, the viral ribonucleoproteins (vRNPs) are released into the cytoplasm of the cell (79). The vRNPs are then transported into the nucleus of the host cell where vRNA and mRNA are both transcribed. After translation, the viral proteins are then exported towards the membrane and the vRNPs are packaged into the new virus before budding off from the host cell. The neuraminidase proteins (NA) finally cleave the bound HA-sialic acid, releasing new viral particles.

Although these viral proteins each have their own individual function that contribute to the infectivity and replication of the virus, they rely on the host factors to function properly. One of the most important host factors that is utilized by the influenza A virus is the SUMOylation cascade (80-82). SUMOylation (Small Ubiquitin-like Modification) is a post-translational modification that is responsible for cell cycle progression, gene regulation, protein stability and protein trafficking (50). The interplay between SUMOylation and the influenza A virus has been documented but the mechanism remains to be completely understood (83-86). The first influenza A virus protein reported to be a SUMO target is the nonstructural protein 1 (NS1), which is involved in a large variety of virus-host interaction and its most prominent function during influenza infection is to antagonize interferon (86, 87).

Here, we investigate the importance of the SUMOylation of NS1 on the replication of the influenza A virus. We applied our qFRET approach to identify the lysine residue

responsible for the SUMOylation of the NS1 protein (37, 58). Current SUMOylation site prediction tools- GPS-SUMO 1.0, SUMOplot™, available at http://abgent.com/sumoplot, and PCI-SUMO- were used to help predict the SUMOylation site of NS1 based on the peptide sequence (88-90). After conducting a site-directed mutagenesis on each lysine residues in NS1, we were able to determine that K131 in the effector domain of NS1 was the SUMO acceptor site. We also developed a fluorescence-based influenza A virus assay and illustrated that growth rate of H1N1 influenza A (A/PR/8/34) with SUMOylation-deficient NS1 protein. Together, these results indicate that NS1 SUMOylation promotes rapid replication of influenza virus, and the interaction of NS1 with SUMOylation components may serve as novel antiviral drug target, due to the well-known function of NS1 for inhibition of host immune responses.

Materials and Methods

Molecular cloning of DNA constructs

The pET28(b) constructs of CyPet-SUMO1, Uba2, Aos1, and Ubc9 were cloned as outlined in (91). The pET 28(b) YPet-Linker 2 construct was made by amplifying the open reading frame of YPet with primers containing NheI and Linker-2 (gtcacctctggttctccgggtctgcaggaatttggtacc) SalI and ligating into a linearized pET28(b) vector (Millipore Corporation, Billerica, MA). After the sequence was verified, the open reading frame of NS1 was amplified via PCR with primers containing SalI and NotI which was ligated into the pET28(b) vector containing YPet-Linker 2 and the sequence was subsequently verified. The mutagenesis of NS1 was performed as outlined in Chapter 13 (92) using Phusion polymerase (New England Biolabs, MA) and tail-to-tail primers designed to introduce site-specific mutations as well as full plasmid amplification. For the lysine-deficient mutant, the mutant YPet-Linker2-NS1 constructs were sequenced and verified that the correct mutations were introduced after every third mutation introduced.

The plasmids used for generation of recombinant influenza virus were first described in (93). In this report, we used ambisense plasmids (pDZ) containing the eight influenza A/Puerto Rico/8/1934 (PR8) viral segments for rescue of a commonly studied laboratory strain, influenza A/Puerto Rico/8/1934 (PR8). Plasmid pDZ-HA with YPet-YPet insert was prepared by creating a NotI restriction site at both ends of the 3' packaging region (45 nucleotides of HA gene coding sequence) and 5' packaging region (80 nucleotides of HA gene coding sequence) of the rescue plasmid pDZ-HA (94). The YPet-YPet insert with a Linker-2 (gtcacctctggttctccgggtctgcaggaatttggtacc) between the two

YPet ORFs was PCR amplified with a NotI restriction site incorporating to both ends, and cloned into the pDZ-HA packaging plasmid with the two packaging regions flanking.

Cell lines

HEK 293 and MDCK cells were cultured in Dulbecco's modified Eagle's medium (GIBCO, Carlsbad, CA), supplemented with 10% fetal bovine serum (GIBCO), penicillin-streptomycin (GIBCO) and 2mM L-Glutamine (GIBCO).

Generation of HA-MDCK cells

MDCK cells were cultured to 90% confluent and transfected with pcDNA3.1-HA using Lipofectamine 2000 (Invitrogen, Carlsbad, CA). Twenty-four hours post transfection, cells were split into 100-mm dishes at low density and selected by the addition of 100 μg/ml hygromycin B (Invitrogen). After visible cell colonies were formed on the dishes, totally 48 cell colonies were picked up and cultured for HA expression screening by western blot. The stable cell line (HA-MDCK) with highest level of HA expression were maintained in medium containing 100 μg/ml hygromycin B.

Protein Expression and Purification

BL21 *E. coli* cells were transformed with the pET28(b) constructs encoding CyPet-SUMO1, Aos1, Uba2, Ubc9, YPet-Linker2-NS1. The transformed *E. coli* was plated onto LB agar plates containing 50 g/mL kanamycin and single colonies were picked up for each unique construct and inoculated into a starter culture. Each starter culture was inoculated into 1 L of 2xYT medium and grown at 37°C, 180 rpm for 3 hrs. Expression of the (6x) His recombinant proteins was induced with 0.6mM IPTG at 25°C, 150 rpm overnight. The bacterial cells were harvested the next day at 4°C, 8,000 rpm. The bacterial

cells were resuspended in 30mL of 20mM Tris-HCl pH 7.4, 500mM NaCl, and 4mM imidazole. The cell suspension was lysed via sonication with an ultrasonic liquid processor (Misonix, Farmingdale, NY). The supernatant was collected after centrifugation at 4°C, 35,000x g for 30 minutes. The recombinant proteins were then bound to Ni^{2+}-NTA agarose beads (QIAGEN, Valencia, CA). The column was washed with sequentially with two column volumes of (WB1), one column volume of (WB2), two column volumes (WB3) and eluted in a buffer containing 20mM Tris-HCl pH 7.4, 200mM NaCl, and 300mM imidazole. The recombinant proteins were dialyzed overnight at 4°C in a buffer containing 20mM Tris-HCl pH 7.4, 50mM NaCl, and 1mM DTT. Protein purity was assessed by SDS-PAGE and Coomassie G-250 staining (Bio-Rad, Hayward, CA), and concentrations were determined by the Bradford assay with known amounts of bovine serum albumin as standards (Thermo-Fisher Scientific Inc., Rockford, IL). Concentration of fluorescent-fusion proteins were determined by their fluorescence.

In silico SUMOylation site identification

The amino acid sequence of the NS1 protein from the influenza A/Puerto Rico/8/1934 was added to the query of each SUMOylation site prediction tool. The GPS-SUMO 1.0 SUMOylation prediction tool was used with a medium SUMOylation threshold for the identification of potential SUMOylated lysine residues. The NS1 sequence was submitted to SUMOplot™, which gave two sites that agreed with previously published results. The NS1 sequence was also submitted to PCI-SUMO tool we picked the lysine residues that overlapped with the GPS-SUMO1 SUMOylation prediction too (88, 90, 95).

FRET-based *in vitro* SUMOylation Assay

To identify the SUMO site of H1N1 NS1, all components of the SUMOylation assay including 1uM CyPet-SUMO1, 50nM Aos1/Uba2, +/- 100nM Ubc9, and 2uM YPet-Linker2-NS1 or its mutants were combined in a buffered solution containing 50 mM Tris–HCl (pH 7.4), 1 mM DTT and 4 mM $MgCl_2$ in a total volume of 60 μL. The sample mixtures were incubated in a Greiner 384-well plate (Sigma-Aldrich) at 37 °C. After adding 1 mM ATP to the sample well the fluorescence emissions were measured in time course using FlexstationII384 (Molecular Devices, Sunnyvale, CA). Emission intensities were measured at three wavelengths: 475 and 530nm given an excitation wavelength of 414nm, and 530nm given an excitation of 475nm.

Em_{FRET} Analysis

The FRET emission values were corrected by subtracting the background from the plate. The real FRET emission (Em_{FRET}) was used to monitor the formation of the SUMO1-NS1 complex, we defined Em_{FRET} as $Em_{FRET} = Em_{total} - \alpha Em_{CyPet} - \beta Em_{Ypet}$ (37). The SUMOylated NS1 product would only be formed when the SUMO E1 and E2 proteins were present with ATP, which would result in an increase in the FRET emission. Mutating the lysine residues on a target protein will result in no increase in FRET emission given SUMO E1, E2 and ATP while the exclusion of any SUMO enzyme or ATP would also result in no increase of FRET. The Em_{FRET} was compared across all time points for each sample for a duration of 25 minutes. The amount of SUMOylated YPet-NS1 and its mutants from different samples were also determined by western blot using anti-NS1 antibody.

Generation of recombinant PR8 virus

The plasmid-based reverse genetic techniques to rescue recombinant influenza viruses have been described previously (93, 96). For the generation of influenza A/Puerto Rico/8/1934 (PR8), a mix of HEK 293 and MDCK cells was first transfected with eight ambisense plasmids (pDZ) containing the eight influenza A/Puerto Rico/8/1934 (PR8) viral segments. Twenty-four hours post transfection, the transfection media was removed, and the transfected cells were cultured in DMEM, 0.3% BSA, 1% PS containing 1 μg/ml of TPCK-trypsin for 48 hours. After 48 hours of changing the media, the supernatant was passaged to infect fresh MDCK cells in 6-well plates. To generate the PR8 viruses with YPet-YPet reporter, the pDZ-HA packaging plasmid with YPet-YPet insert was used in replacement of pDZ-HA for the eight-plasmid transfection on HA-MDCK cells (94).

Growth kinetics of WTPR8, PR8NS1-70A, PR8NS1-70,219A, and PR8NS1-131A viruses in MDCK cells

The viruses were rescued by plasmid DNA as described above. The growth rates of recombinant PR8 viruses with different NS1 mutants were evaluated by infecting MDCK cells in triplicate at a multiplicity of infection (MOI) of 0.001. The inoculum was removed after 60 min of incubation 37°C, washed three times with PBS, and added 2 mL Opti-MEM with 1 ug/ml tosylsulfonyl phenylalanyl chloromethyl ketone (TPCK)-treated trypsin per well. Cells were then further incubated at 37°C. Samples were collected at 12, 24, 36, 48, and 60 h post-infection. The titers of viruses were determined by use of plaque assay in MDCK cells. The growth rates of recombinant PR8 viruses with YPet-YPet reporter and different NS1 mutants were evaluated by infecting HA-MDCK cells in triplicate at a MOI

of 0.001, and after 48 hours incubation the cells were harvested for fluorescence measurement at an excitation wavelength of 475 nm, and emission wavelength of 530 nm.

Plaque Assay

Confluent MDCK cells in 6-well plates were infected with 10-fold dilutions of virus. After a 1-h incubation, the viral inoculum was removed, and the cells were overlaid with 0.65% agar (Oxoid Ltd.) in MEM supplemented with 0.4% BSA, penicillin–streptomycin, 0.01% DEAE dextran and 1ug/mL TPCK-treated trypsin. The plates were incubated for 48 hours at 37°C; then, the agar overlay was removed, and the cells were fixed and stained with 20% methanol and crystal violet. Visualized plaques were counted.

Results

Design of FRET-based approach for SUMOylation site identifications of influenza virus proteins

NS1 of the influenza A virus has been previously identified as a bona fide SUMO target both *in vitro* and *in vivo* (97). To establish a robust system specifically for screening the whole influenza A proteome for SUMOylation targets, we have established a FRET-based *in vitro* SUMOylation assay which serves as a more convenient and sensitive approach compared with traditional western blot-based assays. This approach was first applied to verify the SUMOylation of NS1 and its SUMOylated lysine residues. To this end, we used molecular cloning methods to fuse CyPet and YPet, a pair of engineered fluorescent proteins with enhanced FRET efficiency, to the N-terminus of a mature SUMO1 and NS1, respectively. The approximate peak wavelengths of excitation and emission for CyPet and YPet are Ex 414nm/Em 475nm and Ex 515nm/Em 530 nm, respectively. When the FRET donor (CyPet) and acceptor (YPet) are in close proximity (between 1-10 nm), the excitation of the system at 414nm will cause energy transfer from the excited donor to the acceptor, which results in donor quenching and an increase in acceptor fluorescence. Thus, when CyPet-SUMO1 and YPet-NS1 are mixed in the presence of Aos1/Uba2 (E1), Ubc9 (E2), ATP and other necessary cofactors, if NS1 constitutes a target for SUMOylation then CyPet-SUMO1 can be covalently conjugated to YPet-NS1, resulting in an increase of Em530. On the other hand, if NS1 lacks the ability to be SUMOylation *in vitro*, the fluorescence spectrum of the system will remain the same, as illustrated in Figure 4.1A. This FRET-based SUMOylation assay was performed by

mixing CyPet-SUMO1, YPet-NS1, together with Aos1, Uba2 and Ubc9 proteins in a Tris-buffered system, and after addition of ATP the FRET signal was monitored in real-time. To obtain the absolute FRET emission which is correlate with the amount of bound CyPet-SUMO1 and YPet-NS1, the direct emissions at 530 nm from free Cypet-SUMO1 and Ypet-NS1 need to be determined and subtracted from the total emission intensity at 530 nm. To achieve that, we used a newly developed spectrum analysis described in (37) for determining the absolute FRET signal. In this method, the total fluorescent signal at 530 nm when excited at 414 nm (Em_{total}) is differentiated into three fractions: absolute FRET emission (Em_{FRET}), CyPet direct emission and YPet direct emission. It was found that the direct fluorescence contribution of CyPet at 530 nm is proportional to its emission at 475 nm (FL_{DD}) when excited at CyPet wavelength (414 nm) with a ratio coefficient of x = 0.378, while the direct emission of YPet at 530 nm is proportional to its emission at 530 nm (FL_{AA}) when excited at YPet wavelength (475 nm) with a ratio coefficient y = 0.026.

$$Em_{FRET} = Em_{total} - x * FL_{DD} - y * FL_{AA} \quad (1)$$

Data analysis of real-time Em_{FRET} reveals the kinetics of formation of the isopeptide bond between SUMO1 and NS1 after all SUMOylation components are mixed. Compared with the negative control samples either without Ubc9 or ATP, the sample with all SUMOylation components showed a one-fold increase of Em_{FRET} in 20 min (Figure 4.1B). This proves that influenza A NS1 can be SUMOylated in vitro and the status of CyPet-SUMO1 to YPet-NS1 conjugation can be monitored by absolute FRET in a real-time manner.

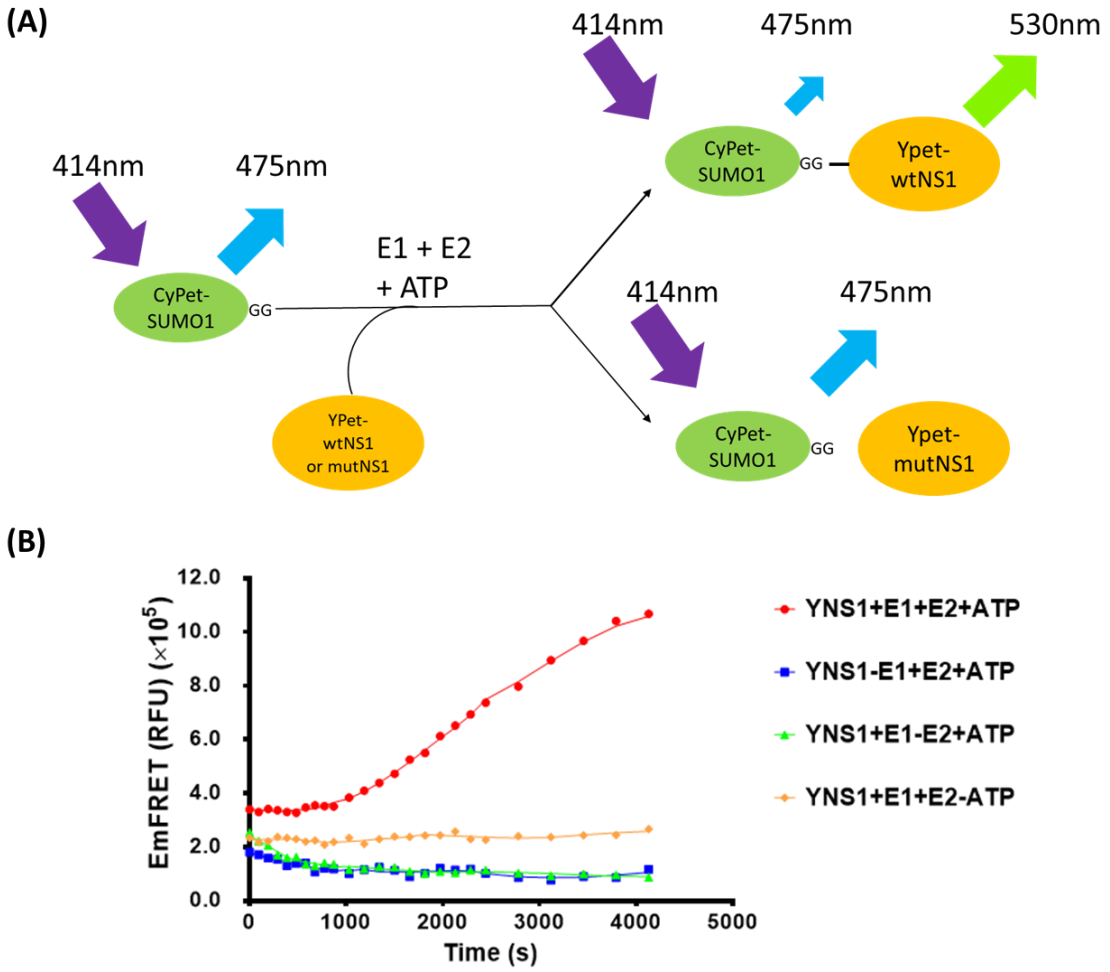

Figure 4.1. Principle of FRET-based SUMOylation assay to determine SUMOylated lysine residues. (A) Scheme of *in vitro* FRET-based SUMOylation assay. If a lysine residue is responsible for SUMOylation, the mutation of the lysine residue to alanine will result in the decrease of the FRET emission at 530 nm given an excitation wavelength of 414 nm. (B) Plot of absolute FRET signal (Em_{FRET}) over time for the reaction mix with different controls. CyPet-SUMO1 and YPet-Linker2-NS1 were added in assay in the presence or absence of SUMO E1, E2, and/or ATP. Em_{FRET} signal was calculated, demonstrating the specificity of the assay for the positive identification of SUMOylated NS1 proteins.

Previous SUMOylation sites of NS1 are not SUMOylated using FRET assay

After we confirmed influenza A virus NS1 protein is a SUMOylation substrate *in vitro*, identification of the SUMO modification sites on NS1 was performed. The cDNA sequence of H1N1 NS1 contains thirteen lysine residues, and it was reported A/Puerto Rico/8/1934 (PR8) NS1 is SUMOylated at K70 and K219 (85). However, our results indicated that mutants of either K70A or K219A or both did not result in reduced SUMOylation compared to the wildtype NS1 (Figure 4.2).

(A)

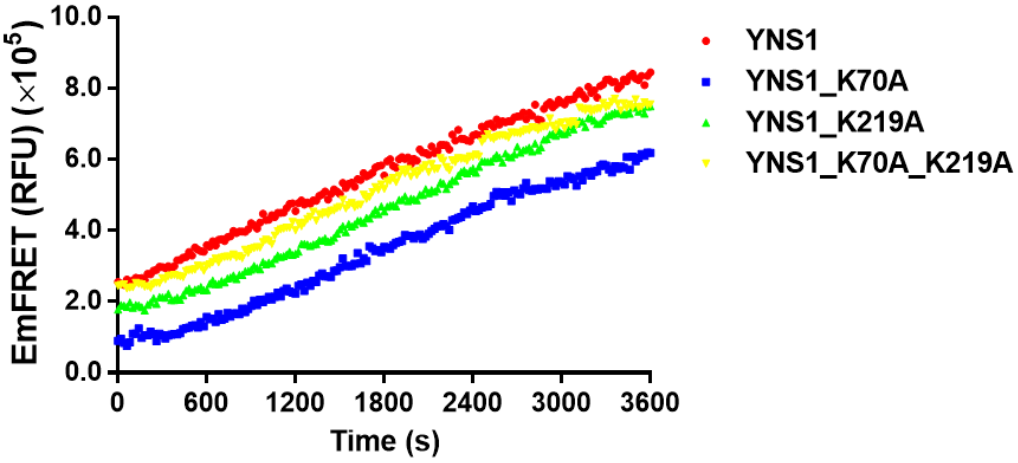
EmFRET (RFU) (×10^5)
10.0
8.0
6.0
4.0
2.0
0.0
0
600
1200
1800
2400
3000
3600
Time (s)
YNS1
YNS1_K70A
YNS1_K219A
YNS1_K70A_K219A

(B)

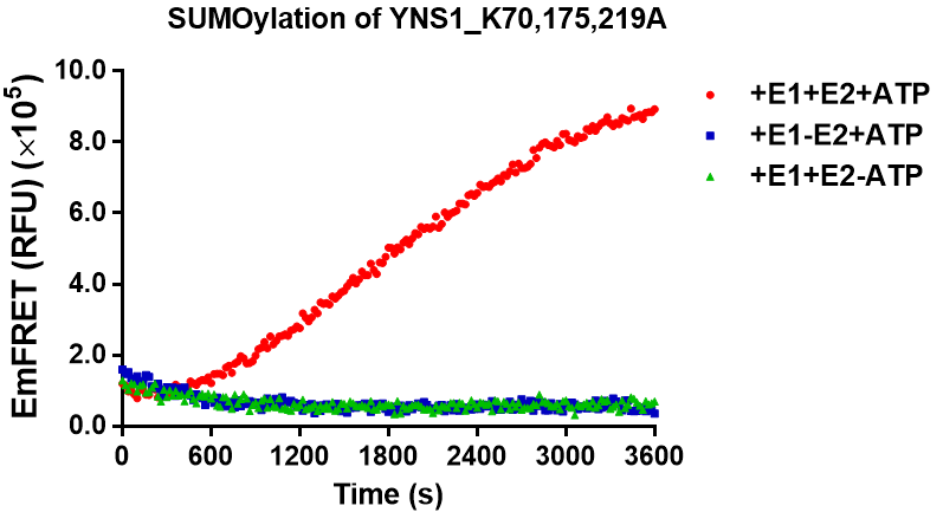
SUMOylation of YNS1_K70,175,219A
EmFRET (RFU) (×10^5)
10.0
8.0
6.0
4.0
2.0
0.0
0
600
1200
1800
2400
3000
3600
Time (s)
+E1+E2+ATP
+E1-E2+ATP
+E1+E2-ATP

Figure 4.2. Establishment of the *in vitro* SUMOylation assay. (A) FRET-based SUMOylation assay with wildtype NS1 and mutant NS1 proteins. NS1 mutants contained lysine residue mutations from previously described SUMOylated lysine residues in NS1. Em_{FRET} increased overtime in the *in vitro* assay demonstrating that these are not the correct SUMOylated lysine residues in NS1. (B) *In vitro* SUMOylation of NS1 mutant determined by the overlap between at least two SUMOylation prediction tools. The triple mutant NS1 K70/175/219A is still SUMOylated which demonstrates the limitation of SUMOylation prediction tools.

Table 4.1: Summary of results for SUMOylated lysine residues based on SUMOylation prediction tools

GPS-SUMO1.0	SUMOplot™	PCI-SUMO
K 70	K 70	K 78
K 175	K 219	K 108
		K 131
		K 175
		K 219

Systematic screening of Lys residues of NS1 for SUMOylation with FRET Assay

We then performed systematic mutagenesis on all possible SUMOylation sites, by introducing one-by-one mutations of all twelve lysine residues accumulatively and investigated the activities of all mutants in the in vitro SUMOylation assay (Table 4.2). The accumulative NS1 mutant #9 still served as active SUMOylation substrate, however NS1 mutant #10 in which K131A was introduced to NS1 mutant #9 completely abolished SUMOylation of the mutant NS1 (Figure 4.3).

(A)

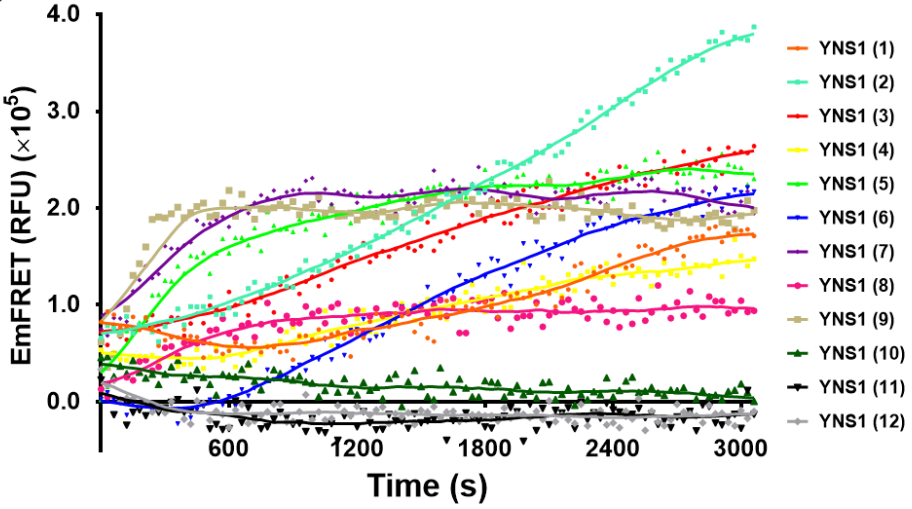
4.0
3.0
2.0
1.0
0.0
EmFRET (RFU) (×10^5)
600
1200
1800
2400
3000
Time (s)
YNS1 (1)
YNS1 (2)
YNS1 (3)
YNS1 (4)
YNS1 (5)
YNS1 (6)
YNS1 (7)
YNS1 (8)
YNS1 (9)
YNS1 (10)
YNS1 (11)
YNS1 (12)

(B)

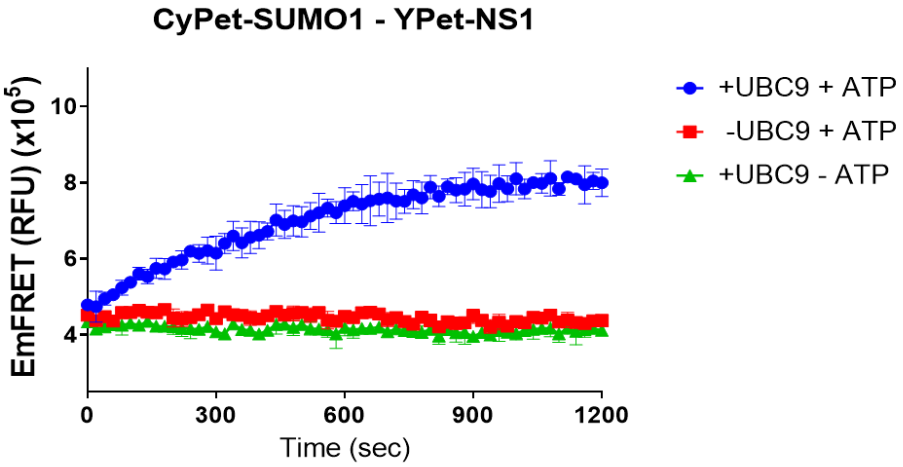
CyPet-SUMO1 - YPet-NS1
10
8
6
4
EmFRET (RFU) (x10^5)
0
300
600
900
1200
Time (sec)
+UBC9 + ATP
-UBC9 + ATP
+UBC9 - ATP

(C)

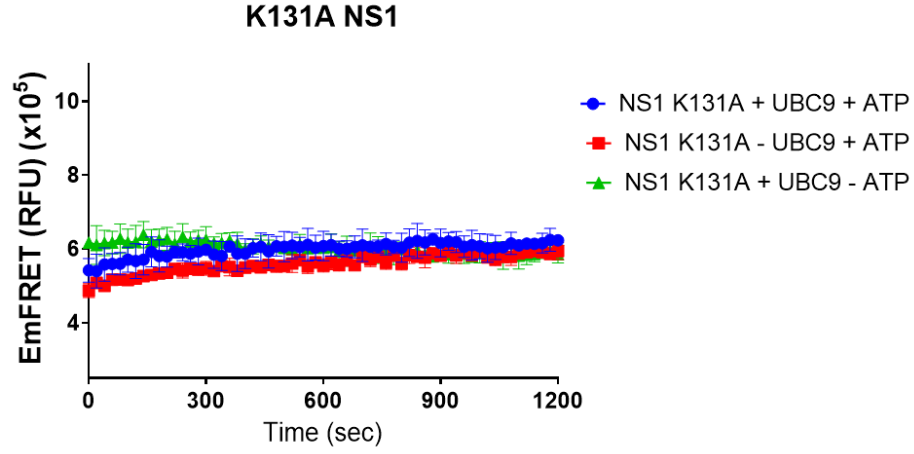
K131A NS1
10
8
6
4
EmFRET (RFU) (x10^5)
0
300
600
900
1200
Time (sec)
NS1 K131A + UBC9 + ATP
NS1 K131A - UBC9 + ATP
NS1 K131A + UBC9 - ATP

Figure 4.3. *In vitro* SUMOylation assay of all mutant YPetNS1. (A) Site-directed mutagenesis of all the lysine residues in NS1, generating a completely lysine-deficient NS1 mutant. Upon the addition of the mutation K131A, there is no increase in Em_{FRET} overtime. (B) Em_{FRET} increases overtime only in the presence of UBC9 and ATP. (C) Em_{FRET} does not increase overtime in the presence or absence of UBC9 and/or ATP when the mutation K131A is introduced to NS1.

Table 4.2. Lysine residues mutated in each mutant YNS1 construct

NS1 Mutant	Lysine Residues mutated to Alanine
1	70
2	175
3	70, 175, 219
4*	70, 108, 175, 217
5	41, 70, 108, 175, 217
6	41, 62, 70, 126, 108, 175, 217
7*	41, 62, 78, 126, 108, 175, 217
8	20, 41, 62, 78, 126, 108, 175, 217
9	20, 41, 62, 78, 108, 110, 126, 175, 217
10	20, 41, 62, 78, 108, 110, 126, 131, 175, 217
11	20, 41, 62, 78, 108, 110, 126, 131, 175, 217, 219
12	20, 41, 62, 70, 78, 108, 110, 126, 131, 175, 217, 219

Confirmation of NS1 131 as SUMOylation site

A mutant NS1 with single site mutation K131A was created and examined, and it displayed a significant loss of SUMOylation compared to wildtype NS1. Additional FRET-based SUMOylation assay and western blot were performed to confirm that Lys-131 is the only SUMOylation site of H1N1 NS1, rather than Lys 70 and Lys 219 (Figure 4.4).

(A)

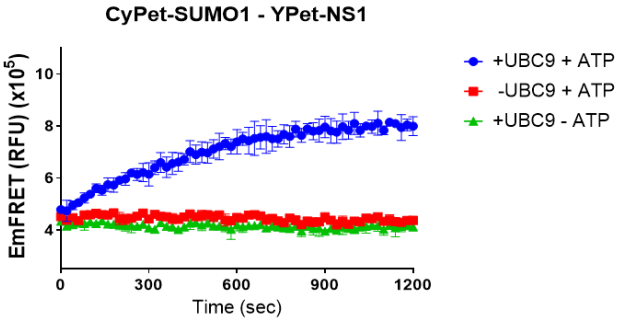
CyPet-SUMO1 - YPet-NS1
EmFRET (RFU) (x10^5)
10
8
6
4
0
300
600
900
1200
Time (sec)
+UBC9 + ATP
-UBC9 + ATP
+UBC9 - ATP

(B)

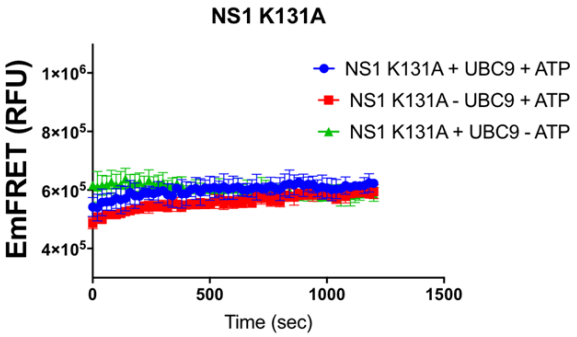
NS1 K131A
EmFRET (RFU)
1×10^6
8×10^5
6×10^5
4×10^5
0
500
1000
1500
Time (sec)
NS1 K131A + UBC9 + ATP
NS1 K131A - UBC9 + ATP
NS1 K131A + UBC9 - ATP

(C)

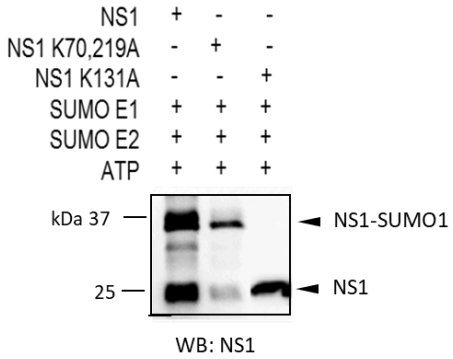
NS1 + - -
NS1 K70,219A - + -
NS1 K131A - - +
SUMO E1 + + +
SUMO E2 + + +
ATP + + +
kDa 37
25
NS1-SUMO1
NS1
WB: NS1

(D)

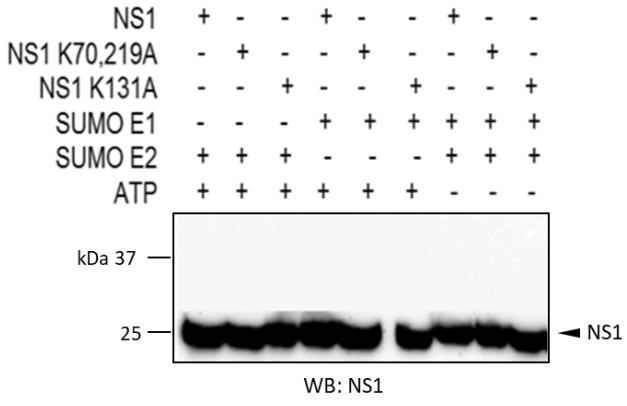
NS1 + - - + - - + - -
NS1 K70,219A - + - - + - - + -
NS1 K131A - - + - - + - - +
SUMO E1 - - - + + + + + +
SUMO E2 + + + - - - + + +
ATP + + + + + + - - -
kDa 37
25
NS1
WB: NS1

Figure 4.4. Confirmation of the SUMOylation site of NS1. (A) FRET-based assay of CyPet-SUMO1 and YPet-NS1 in the presence or absence of SUMO E1, E2, and/or ATP. The increase in Em_{FRET} is specific to the SUMOylation of NS1. (B) FRET-based SUMOylation assay of a mutant NS1 with the lysine residue 131 mutated to alanine. In the presence or absence of SUMO E2 and/or ATP, NS1 cannot be SUMOylated. (C) SUMOylation of NS1 in vitro. Mature SUMO1 and SUMO E1, E2, and ATP were added with NS1 and mutant NS1 proteins with specific lysine residues mutated to alanine. (D) SUMOylation assays of NS1 and NS1 mutants in the presence of absence of SUMO E1, SUMO E2, or ATP. Western blots were probed with anti-NS1. The positions of molecular mass standards are marked on the left.

The significance of SUMOylation site of NS1 131 in influenza virus replication

The non-structural (NS1) protein of influenza A is an important multifunctional factor that plays diverse roles in viral life cycle. Among its multiple functions, the major effect of NS1 is its inhibition of host interferon-stimulated immune response. It was also shown that knockdown of Ubc9 in host cells reduce influenza A virus replication, which indicated overall SUMOylation is important for influenza A virus production (98). Here, we studied whether NS1 K131 was the essential SUMOylation site for influenza A virus growth. To address this question, we developed a double-fluorescent reporter strategy to track the virus replication, and we compared this parameter together with titer of the released viruses on A/Puerto Rico/8/1934 (PR8) strains with different NS1 mutants (Figure 4.5A, B). In this strategy, we put a YPet-YPet gene in the middle of HA gene and still kept the signal regions on both ends that can help package the vRNA into viral particles (94). And the expression level of YPet-YPet reporter is correlated to the amounts of virions replicated in host cells. Both parameters showed significant drop in terms of virus replication when compared H1N1_NS1 K131A with H1N1_wt NS1, which proved SUMOylation on NS1 K131 is critical in influenza A virus life cycle (Figure 4.5C).

To confirm whether these mutations affect influenza virus replication, we also compared the multicycle growth of wild-type PR8 and two NS1 mutation viruses in MDCK cells with low MOI (0.001) through traditional plaque assay. All of these three viruses were able to replicate; however, the viral titers in PR8NS1-131A-infected cells were significantly lower than those in the WTPR8- and PR8NS1-70A-infected cells at 36, 48,

and 60 h post infection (Figure 4.6). These results validate NS1-131A affects influenza replication.

(A)

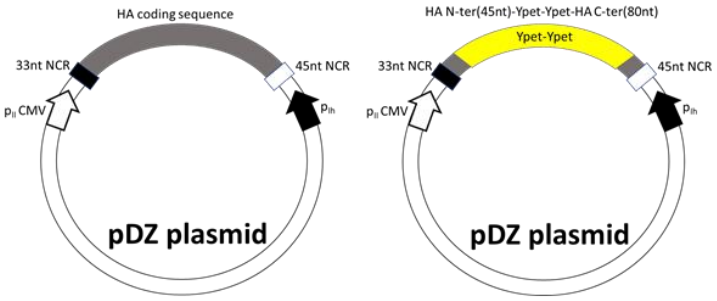
HA coding sequence
33nt NCR
45nt NCR
pDZ plasmid
HA N-ter(45nt)-Ypet-Ypet-HA C-ter(80nt)
Ypet-Ypet
33nt NCR
45nt NCR
pDZ plasmid

(B)

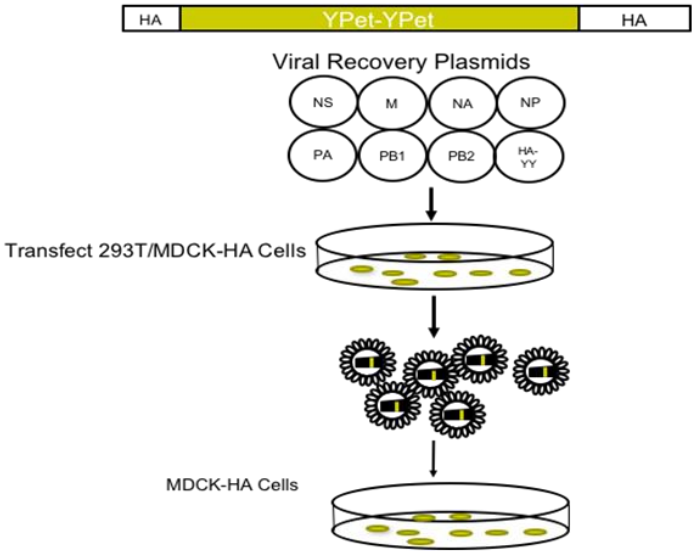
HA
YPet-YPet
HA
Viral Recovery Plasmids
NS
M
NA
NP
PA
PB1
PB2
HA-YY
Transfect 293T/MDCK-HA Cells
MDCK-HA Cells

(C)

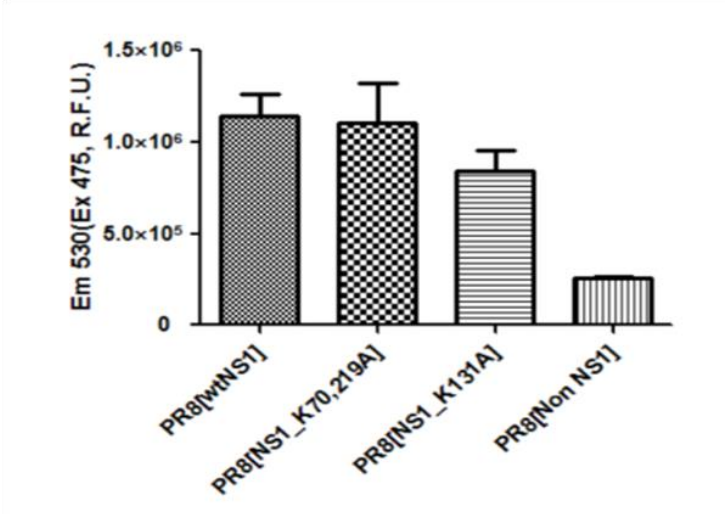
Em 530(Ex 475, R.F.U.)
1.5×10⁶
1.0×10⁶
5.0×10⁵
0
PR8[wtNS1]
PR8[NS1_K70,219A]
PR8[NS1_K131A]
PR8[Non NS1]

Figure 4.5. Generation of HA-pseudotyped Ypet-Ypet-expressing influenza viruses.

(A) Plasmid design with 2x tandem Ypet incorporated in a pDZ-HA encoding plasmid. (B) Viral rescue. HEK 293T/MDCK-HA coculture was transfected with ambisense pDZ plasmids (PB2, PB1, PA, NA, NP, M, NS) and HA-YPet-YPet pDZ plasmid. The transfection medium was exchanged with infection medium after 24 hours. After 48 hours of growth in the infection medium, infection medium was passaged to fresh HA MDCK-expressing cells and virus rescue was confirmed by YPet fluorescence. (C) Fluorescence assay of HA-YPet-YPet influenza with NS1 mutants. Wildtype NS1 PR8 and NS1 K70/219A PR8 have distinctly more fluorescence than NS1 K131A PR8 and a pDZ plasmid containing no gene.

(A)

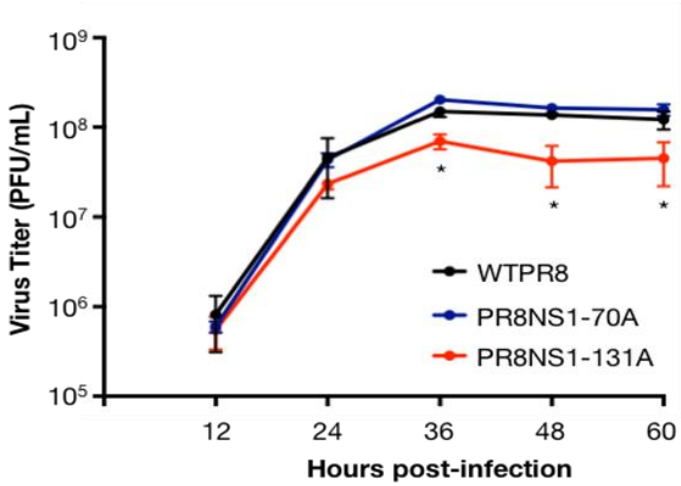

(B)

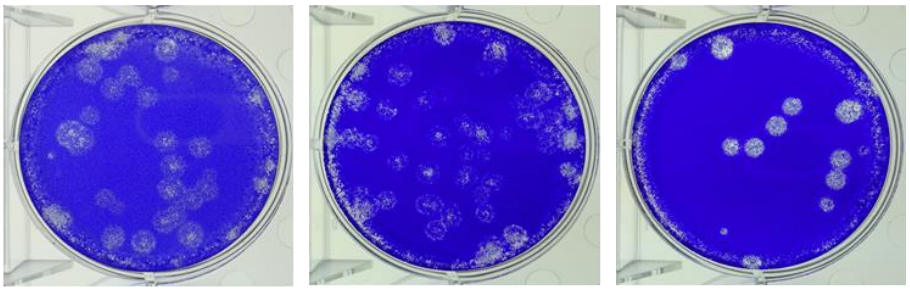

Figure 4.6. Virus replication kinetics in MDCK cells by plaque assay. (A) MDCK cells were infected in triplicate with viruses containing wildtype or mutant NS1 gene at MOI of 0.001. The samples were collected at 12, 24, 36, 48, 60h post-infection, and viral titers were determined by plaque assay in MDCK cells. (B) Comparison of numbers of visualized plaques of viruses containing wildtype or mutant NS1 gene in MDCK cells.

Discussion

Despite the substantial knowledge of structure and molecular function of each influenza viral protein during infection, the mechanism of how influenza virus hijacks the host cell's machinery for their own benefit is still being deciphered. SUMOylation has been reported as one of the top five host factors (80, 81) responsible for aiding viral replication. However, the specific interactions between SUMOylation and the influenza A virus, driven by the direct SUMOylation of viral proteins is being characterized. The non-structural protein (NS1) of influenza A virus is a critical virulence factor during viral infection. The major function related to NS1 is its neutralization of interferon-stimulated host immune responses, besides that NS1 has multiple accessory functions within infected cells, including enhancement of viral RNA translation and viral protein synthesis, and blocking cellular mRNA maturation. Pal et al. were the first to identify influenza A viral protein NS1 to be a *bona fide* SUMOylation target, which supports that SUMOylation is likely to serve as a key regulator for virus replication (97). Xu et al. confirmed the direct SUMOylation of NS1 and further mapped the SUMOylation sites to be located at C-terminal of NS1. They also showed that SUMOylation of NS1 enhances the stability of NS1 protein and thus increases virus titers in host cells (86). More recently, Santos et al. identified the main SUMOylation sites in A/Puerto Rico/8/1934 (PR8) NS1 to be residues K219 and K70, and demonstrated the SUMOylation-deficient form of NS1 diminishes its ability to antagonize cellular IFN response (85). Here, we have developed a novel sensitive FRET-based SUMOylation assay and found NS1_K70A_K219A from A/Puerto Rico/8/1934 (PR8) was SUMOylated at relatively the same level as wt_NS1. Therefore,

we did systematic mutagenesis on each of all lysine residues in NS1 and mapped the SUMO acceptor site to be residue K131.

The traditional method to determine virus titers by plaque assay is tedious and non-accurate. Recently, a fluorescent reporter strategy has been developed for influenza virus assay and we adapted this strategy to a more sensitive double-fluorescent reporter strategy (94). In this method, we inserted a YPet-YPet fluorescent tag in the middle of influenza HA vRNA and kept the signal regions on both ends which can help package the vRNA into viral particles. Thus, if the virions can be replicated then the fluorescent protein would be translated at a corresponding level which is indicative of virus growth rate. We have proven by this method that growth of SUMOylation-deficient PR8 virus mutant with NS1_K131A was significantly decreased indicated by attenuated fluorescent signal from infected host cells compared to virus with wt_NS1 or NS1_K70A_K219A, which suggests a critical role of NS1 SUMOylation for enhancing influenza virus replication. The SUMOylated lysine residues in the NS1 protein were previously identified by Pal et al as K70 and K219 however, we have found that the sole lysine residue responsible for the SUMOylation of NS1 is K131. When we mutated K131 to alanine (K131A) in NS1 and recovered virus, there was a decrease in the fluorescence of the virus, indicating that the SUMOylation of NS1 is important but not essential for the replication of the influenza A virus. The results of a SUMOylation-deficient NS1 mutant agree with S. Pal et al but only for our K131A mutant.

Förster resonance energy transfer (FRET) is a widely used technique in biological research for its high sensitivity and specificity. Here, we have developed FRET-based

SUMOylation assay which has several advantages over traditional methods for determining the SUMOylation site. First, FRET signal is highly proportional to the number of molecular interaction events, thus this approach can accurately determine the amounts of interactive partners quantitatively. Previous methods used to determine the SUMOylation site of proteins involved Co-IP which has a limit of detection based upon the abundance of the protein in the sample and the affinity of the antibodies towards the epitopes. The embedded epitope in target protein when conjugated with other protein or nonspecific recognition of antibody to other host protein can easily cause false positive or false negative results. Also, FRET signal can be monitored in real time which can provide kinetics information to compare between the SUMOylation targets with different site mutations. This method does not depend on antibodies which can have different affinities for the target epitope and we are able to use proteins that have not been completely purified. Moreover, this method is straightforward and protein modification with fluorescent proteins can be easily achieved by molecular cloning.

Viral proteins engage with the host's SUMO modifications in a variety of ways, through which the virus can hijack the cellular SUMOylation pathway for their benefit or evade host antiviral response. SUMOylation has been shown to positively regulate wild-type influenza A virus infection, as evidenced by a global increase in SUMOylation events during influenza infection (84, 85), and decrease of influenza viral replication rate after knocking down host SUMO E2-Ubc9 (98). Our results demonstrate that a NS1 SUMOylation-deficient PR8 virus has lower viral replication rate in infected cells compared to that of wild-type virus, which indicates SUMOylation of NS1 may have

functional consequences. It was reported that NS1 SUMOylation enhances the stability of NS1 protein (86). On the contrary, Santos et al. reported that SUMOylation has no effect on the cellular localization or the stability of NS1, instead SUMO modification regulates the proportion of NS1 dimers and polymers in host cells (85).

Although it is widely believed the cellular SUMOylation is critical for efficient influenza virus growth and infection, the direct importance of SUMOylation for influenza infection remains mostly unexplored. Here, we report SUMOylation of residue K131 of influenza NS1 is important but not essential for influenza virus replication. We expect to find other SUMOylation sites in other influenza viral proteins, which are likely to expand their functional activities. Our FRET-based assay provides the advantage for large-scale SUMOylation site screening from the whole influenza proteomics, since it can be easily converted into a high-throughput format.

The influenza virus remains a major threat to human health at a global level, due to its considerable morbidity. The current available two classes of antiviral drugs that target M2 (amantadine and rimantadine) and NA (oseltamivir and zanamivir) have limited effectiveness due to the emergence of drug-resistant strains. An alternative approach for developing novel antiviral drugs is to target host factors that are essential for viral replication. Given the critical role of SUMOylation pathway for efficient influenza infection, the development of inhibitors that block SUMOylation on viral proteins might provide future antivirals that can effectively treat drug-resistant strains. Efforts in this direction can also increase our knowledge of the functional interactions between SUMOylation and viral proteins.

REFERENCES

1. Hershko A & Ciechanover A (1998) The ubiquitin system. *Annu Rev Biochem* 67:425-479.

2. Bayer P, *et al.* (1998) Structure determination of the small ubiquitin-related modifier SUMO-1. *J Mol Biol* 280(2):275-286.

3. Johnson ES (2004) Protein modification by SUMO. *Annu Rev Biochem* 73:355-382.

4. Desterro JM, Rodriguez MS, & Hay RT (1998) SUMO-1 modification of IkappaBalpha inhibits NF-kappaB activation. *Mol Cell* 2(2):233-239.

5. Steffan JS, *et al.* (2004) SUMO modification of Huntingtin and Huntington's disease pathology. *Science* 304(5667):100-104.

6. Colombo R, Boggio R, Seiser C, Draetta GF, & Chiocca S (2002) The adenovirus protein Gam1 interferes with sumoylation of histone deacetylase 1. *EMBO Rep* 3(11):1062-1068.

7. Lois LM & Lima CD (2005) Structures of the SUMO E1 provide mechanistic insights into SUMO activation and E2 recruitment to E1. *EMBO J* 24(3):439-451.

8. Tatham MH, *et al.* (2005) Unique binding interactions among Ubc9, SUMO and RanBP2 reveal a mechanism for SUMO paralog selection. *Nat Struct Mol Biol* 12(1):67-74.

9. Tang Z, Hecker CM, Scheschonka A, & Betz H (2008) Protein interactions in the sumoylation cascade: lessons from X-ray structures. *FEBS J* 275(12):3003-3015.

10. Bohren KM, Nadkarni V, Song JH, Gabbay KH, & Owerbach D (2004) A M55V polymorphism in a novel SUMO gene (SUMO-4) differentially activates heat shock transcription factors and is associated with susceptibility to type I diabetes mellitus. *J Biol Chem* 279(26):27233-27238.

11. Palvimo JJ (2007) PIAS proteins as regulators of small ubiquitin-related modifier (SUMO) modifications and transcription. *Biochem Soc Trans* 35(Pt 6):1405-1408.

12. Chung CD, *et al.* (1997) Specific inhibition of Stat3 signal transduction by PIAS3. *Science* 278(5344):1803-1805.

13. Liu B, *et al.* (1998) Inhibition of Stat1-mediated gene activation by PIAS1. *Proc Natl Acad Sci U S A* 95(18):10626-10631.

14. Ungureanu D, *et al.* (2003) PIAS proteins promote SUMO-1 conjugation to STAT1. *Blood* 102(9):3311-3313.

15. Schmidt D & Muller S (2002) Members of the PIAS family act as SUMO ligases for c-Jun and p53 and repress p53 activity. *Proc Natl Acad Sci U S A* 99(5):2872-2877.

16. Nacerddine K, *et al.* (2005) The SUMO pathway is essential for nuclear integrity and chromosome segregation in mice. *Developmental cell* 9(6):769-779.

17. Alkuraya FS, *et al.* (2006) SUMO1 haploinsufficiency leads to cleft lip and palate. *Science (New York, N.Y.)* 313(5794):1751.

18. Liu B, *et al.* (2004) PIAS1 selectively inhibits interferon-inducible genes and is important in innate immunity. *Nature immunology* 5(9):891-898.

19. Vassilev LT, *et al.* (2004) In vivo activation of the p53 pathway by small-molecule antagonists of MDM2. *Science* 303(5659):844-848.

20. Saucerman JJ, *et al.* (2006) Systems analysis of PKA-mediated phosphorylation gradients in live cardiac myocytes. *Proc Natl Acad Sci U S A* 103(34):12923-12928.

21. Gordon GW, Berry G, Liang XH, Levine B, & Herman B (1998) Quantitative fluorescence resonance energy transfer measurements using fluorescence microscopy. *Biophys J* 74(5):2702-2713.

22. Dams G, *et al.* (2007) A time-resolved fluorescence assay to identify small-molecule inhibitors of HIV-1 fusion. *J Biomol Screen* 12(6):865-874.

23. Nguyen AW & Daugherty PS (2005) Evolutionary optimization of fluorescent proteins for intracellular FRET. *Nat Biotechnol* 23(3):355-360.

24. Gilson MK & Zhou HX (2007) Calculation of protein-ligand binding affinities. *Annual review of biophysics and biomolecular structure* 36:21-42.

25. Boozer C, Kim G, Cong S, Guan H, & Londergan T (2006) Looking towards label-free biomolecular interaction analysis in a high-throughput format: a review of new surface plasmon resonance technologies. *Current opinion in biotechnology* 17(4):400-405.

26. Homola J (2008) Surface plasmon resonance sensors for detection of chemical and biological species. *Chemical reviews* 108(2):462-493.

27. Freire E, van Osdol WW, Mayorga OL, & Sanchez-Ruiz JM (1990) Calorimetrically determined dynamics of complex unfolding transitions in proteins. *Annual review of biophysics and biophysical chemistry* 19:159-188.

28. Perozzo R, Folkers G, & Scapozza L (2004) Thermodynamics of protein-ligand interactions: history, presence, and future aspects. *Journal of receptor and signal transduction research* 24(1-2):1-52.

29. Seeman P, Corbett R, & Van Tol HH (1997) Atypical neuroleptics have low affinity for dopamine D2 receptors or are selective for D4 receptors. *Neuropsychopharmacology : official publication of the American College of Neuropsychopharmacology* 16(2):93-110; discussion 111-135.

30. Gill G (2004) SUMO and ubiquitin in the nucleus: different functions, similar mechanisms? *Genes & development* 18(17):2046-2059.

31. Olsen SK, Capili AD, Lu X, Tan DS, & Lima CD (2010) Active site remodelling accompanies thioester bond formation in the SUMO E1. *Nature* 463(7283):906-912.

32. Meulmeester E, Kunze M, Hsiao HH, Urlaub H, & Melchior F (2008) Mechanism and consequences for paralog-specific sumoylation of ubiquitin-specific protease 25. *Molecular cell* 30(5):610-619.

33. Rytinki MM, Kaikkonen S, Pehkonen P, Jaaskelainen T, & Palvimo JJ (2009) PIAS proteins: pleiotropic interactors associated with SUMO. *Cellular and molecular life sciences : CMLS* 66(18):3029-3041.

34. Yang SH, Jaffray E, Hay RT, & Sharrocks AD (2003) Dynamic interplay of the SUMO and ERK pathways in regulating Elk-1 transcriptional activity. *Molecular cell* 12(1):63-74.

35. Liao JY, Song Y, & Liu Y (2015) A new trend to determine biochemical parameters by quantitative FRET assays. *Acta pharmacologica Sinica* 36(12):1408-1415.

36. Martin SF, Tatham MH, Hay RT, & Samuel ID (2008) Quantitative analysis of multi-protein interactions using FRET: application to the SUMO pathway. *Protein science : a publication of the Protein Society* 17(4):777-784.

37. Song Y, Madahar V, & Liao J (2011) Development of FRET assay into quantitative and high-throughput screening technology platforms for protein-protein interactions. *Annals of biomedical engineering* 39(4):1224-1234.

38. Song Y, Rodgers VG, Schultz JS, & Liao J (2012) Protein interaction affinity determination by quantitative FRET technology. *Biotechnology and bioengineering* 109(11):2875-2883.

39. Tatham MH, Chen Y, & Hay RT (2003) Role of two residues proximal to the active site of Ubc9 in substrate recognition by the Ubc9.SUMO-1 thiolester complex. *Biochemistry* 42(11):3168-3179.

40. Tatham MH, *et al.* (2003) Role of an N-terminal site of Ubc9 in SUMO-1, -2, and -3 binding and conjugation. *Biochemistry* 42(33):9959-9969.

41. Cho W, Bittova L, & Stahelin RV (2001) Membrane binding assays for peripheral proteins. *Anal Biochem* 296(2):153-161.

42. Schuck P & Minton AP (1996) Analysis of mass transport-limited binding kinetics in evanescent wave biosensors. *Anal Biochem* 240(2):262-272.

43. Nieba L, Krebber A, & Pluckthun A (1996) Competition BIAcore for measuring true affinities: large differences from values determined from binding kinetics. *Anal Biochem* 234(2):155-165.

44. O'Shannessy DJ & Winzor DJ (1996) Interpretation of deviations from pseudo-first-order kinetic behavior in the characterization of ligand binding by biosensor technology. *Anal Biochem* 236(2):275-283.

45. Baker SF, Othman R, & Wilton DC (1998) Tryptophan-containing mutant of human (group IIa) secreted phospholipase A2 has a dramatically increased ability to hydrolyze phosphatidylcholine vesicles and cell membranes. *Biochemistry* 37(38):13203-13211.

46. Han SK, *et al.* (1999) Roles of Trp31 in high membrane binding and proinflammatory activity of human group V phospholipase A2. *J Biol Chem* 274(17):11881-11888.

47. Gelb MH, Cho W, & Wilton DC (1999) Interfacial binding of secreted phospholipases A(2): more than electrostatics and a major role for tryptophan. *Curr Opin Struct Biol* 9(4):428-432.

48. Sumandea M, Das S, Sumandea C, & Cho W (1999) Roles of aromatic residues in high interfacial activity of Naja naja atra phospholipase A2. *Biochemistry* 38(49):16290-16297.

49. Bernier-Villamor V, Sampson DA, Matunis MJ, & Lima CD (2002) Structural basis for E2-mediated SUMO conjugation revealed by a complex between ubiquitin-conjugating enzyme Ubc9 and RanGAP1. *Cell* 108(3):345-356.

50. Everett RD, Boutell C, & Hale BG (2013) Interplay between viruses and host sumoylation pathways. *Nature reviews. Microbiology* 11(6):400-411.

51. Sarge KD & Park-Sarge OK (2009) Sumoylation and human disease pathogenesis. *Trends in biochemical sciences* 34(4):200-205.

52. Fukuda I, *et al.* (2009) Ginkgolic acid inhibits protein SUMOylation by blocking formation of the E1-SUMO intermediate. *Chemistry & biology* 16(2):133-140.

53. Fukuda I, *et al.* (2009) Kerriamycin B inhibits protein SUMOylation. *The Journal of antibiotics* 62(4):221-224.

54. Yang X, Zhu W, Chen J, Qian Z, & Xie J (2004) [Study on anti-bacterium activity of ginkgolic acids and their momomers]. *Zhong yao cai = Zhongyaocai = Journal of Chinese medicinal materials* 27(9):661-663.

55. Bogachek MV, *et al.* (2014) Sumoylation pathway is required to maintain the basal breast cancer subtype. *Cancer cell* 25(6):748-761.

56. Kim YS, Nagy K, Keyser S, & Schneekloth JS, Jr. (2013) An electrophoretic mobility shift assay identifies a mechanistically unique inhibitor of protein sumoylation. *Chemistry & biology* 20(4):604-613.

57. Tossidou I, Himmelseher E, Teng B, Haller H, & Schiffer M (2014) SUMOylation determines turnover and localization of nephrin at the plasma membrane. *Kidney international* 86(6):1161-1173.

58. Jiang L, *et al.* (2013) Internal calibration Forster resonance energy transfer assay: a real-time approach for determining protease kinetics. *Sensors* 13(4):4553-4570.

59. Liu Y, Song Y, Madahar V, & Liao J (2012) Quantitative Forster resonance energy transfer analysis for kinetic determinations of SUMO-specific protease. *Analytical biochemistry* 422(1):14-21.

60. Wiryawan H, Dan K, Etuale M, Shen Y, & Liao J (2015) Determination of SUMO1 and ATP affinity for the SUMO E1by quantitative FRET technology. *Biotechnology and bioengineering* 112(4):652-658.

61. Cantor CR & Schimmel PR (1980) *Biophysical chemistry: Part III: the behavior of biological macromolecules* (Macmillan).

62. Chance B (1991) Optical method. *Annual review of biophysics and biophysical chemistry* 20(1):1-30.

63. Dewey TG (1991) *Biophysical and biochemical aspects of fluorescence spectroscopy* (Springer).

64. Taylor F (1985) Flow-through pH-stat method for lipase activity. *Analytical biochemistry* 148(1):149-153.

65. Walters DE (2002) Enzymes. A Practical Introduction to Structure, Mechanism, and Data Analysis. Second Edition By Robert A. Copeland. Wiley-VCH, New York. 2000. xvi + 397 pp. 16 × 24.5 cm. ISBN 0-471-35929-7. $99.95. *Journal of Medicinal Chemistry* 45(25):5607-5607.

66. Whiteley CG (2000) Mechanistic and kinetic studies of inhibition of enzymes. *Cell biochemistry and biophysics* 33(3):217-225.

67. Kakkar T, Boxenbaum H, & Mayersohn M (1999) Estimation of Ki in a competitive enzyme-inhibition model: comparisons among three methods of data analysis. *Drug metabolism and disposition: the biological fate of chemicals* 27(6):756-762.

68. Kakkar T, Pak Y, & Mayersohn M (2000) Evaluation of a minimal experimental design for determination of enzyme kinetic parameters and inhibition mechanism. *The Journal of pharmacology and experimental therapeutics* 293(3):861-869.

69. Song Y & Liao J (2012) An in vitro Forster resonance energy transfer-based high-throughput screening assay for inhibitors of protein-protein interactions in SUMOylation pathway. *Assay and drug development technologies* 10(4):336-343.

70. Lineweaver H & Burk D (1934) The Determination of Enzyme Dissociation Constants. *Journal of the American Chemical Society* 56(3):658-666.

71. Dixon M (1953) The determination of enzyme inhibitor constants. *The Biochemical journal* 55(1):170-171.

72. Nimmo IA & Atkins GL (1976) Methods for fitting equations with two or more non-linear parameters. *Biochemical Journal* 157(2):489.

73. Brassard P, *et al.* (2017) The effect of statins on influenza-like illness morbidity and mortality. *Pharmacoepidemiology and drug safety* 26(1):63-70.

74. Kuiken T, *et al.* (2006) Host species barriers to influenza virus infections. *Science (New York, N.Y.)* 312(5772):394-397.

75. Nair H, *et al.* (2011) Global burden of respiratory infections due to seasonal influenza in young children: a systematic review and meta-analysis. *Lancet (London, England)* 378(9807):1917-1930.

76. Thompson WW, *et al.* (2009) Estimates of US influenza-associated deaths made using four different methods. *Influenza and other respiratory viruses* 3(1):37-49.

77. Stencel-Baerenwald JE, Reiss K, Reiter DM, Stehle T, & Dermody TS (2014) The sweet spot: defining virus-sialic acid interactions. *Nature reviews. Microbiology* 12(11):739-749.

78. Samji T (2009) Influenza A: understanding the viral life cycle. *The Yale journal of biology and medicine* 82(4):153-159.

79. Bouvier NM & Palese P (2008) The biology of influenza viruses. *Vaccine* 26 Suppl 4:D49-53.

80. Karlas A, *et al.* (2010) Genome-wide RNAi screen identifies human host factors crucial for influenza virus replication. *Nature* 463(7282):818-822.

81. Konig R, *et al.* (2010) Human host factors required for influenza virus replication. *Nature* 463(7282):813-817.

82. Shapira SD, *et al.* (2009) A physical and regulatory map of host-influenza interactions reveals pathways in H1N1 infection. *Cell* 139(7):1255-1267.

83. Han Q, *et al.* (2014) Sumoylation of influenza A virus nucleoprotein is essential for intracellular trafficking and virus growth. *Journal of virology* 88(16):9379-9390.

84. Pal S, Santos A, Rosas JM, Ortiz-Guzman J, & Rosas-Acosta G (2011) Influenza A virus interacts extensively with the cellular SUMOylation system during infection. *Virus research* 158(1-2):12-27.

85. Santos A, *et al.* (2013) SUMOylation affects the interferon blocking activity of the influenza A nonstructural protein NS1 without affecting its stability or cellular localization. *Journal of virology* 87(10):5602-5620.

86. Xu K, *et al.* (2011) Modification of nonstructural protein 1 of influenza A virus by SUMO1. *Journal of virology* 85(2):1086-1098.

87. Killip MJ, Fodor E, & Randall RE (2015) Influenza virus activation of the interferon system. *Virus research* 209:11-22.

88. Green J, Dmochowski G, & Golshani A (2006) *Prediction Of Protein Sumoylation Sites Via Parallel Cascade Identification*.

89. Yavuz AS & Sezerman U (2010) SUMOtr: SUMOylation site prediction based on 3D structure and hydrophobicity. *2010 5th International Symposium on Health Informatics and Bioinformatics*, pp 93-97.

90. Zhao Q, *et al.* (2014) GPS-SUMO: a tool for the prediction of sumoylation sites and SUMO-interaction motifs. *Nucleic acids research* 42(Web Server issue):W325-330.

91. Song Y & Liao J (2012) Systematic determinations of SUMOylation activation intermediates and dynamics by a sensitive and quantitative FRET assay. *Molecular bioSystems* 8(6):1723-1729.

92. Hsieh P-C & Vaisvila R (2013) Protein Engineering: Single or Multiple Site-Directed Mutagenesis. *Enzyme Engineering: Methods and Protocols*, ed Samuelson JC (Humana Press, Totowa, NJ), pp 173-186.

93. Fodor E, *et al.* (1999) Rescue of influenza A virus from recombinant DNA. *Journal of virology* 73(11):9679-9682.

94. Marsh GA, Hatami R, & Palese P (2007) Specific residues of the influenza A virus hemagglutinin viral RNA are important for efficient packaging into budding virions. *Journal of virology* 81(18):9727-9736.

95. Jones DT (1999) Protein secondary structure prediction based on position-specific scoring matrices. *Journal of molecular biology* 292(2):195-202.

96. Martinez-Sobrido L & Garcia-Sastre A (2010) Generation of recombinant influenza virus from plasmid DNA. *Journal of visualized experiments : JoVE* (42).

97. Pal S, Rosas JM, & Rosas-Acosta G (2010) Identification of the non-structural influenza A viral protein NS1A as a bona fide target of the Small Ubiquitin-like MOdifier by the use of dicistronic expression constructs. *Journal of virological methods* 163(2):498-504.

98. Wu CY, Jeng KS, & Lai MM (2011) The SUMOylation of matrix protein M1 modulates the assembly and morphogenesis of influenza A virus. *Journal of virology* 85(13):6618-6628.